evidenced by immunohistochemical and Western blotting analyses (Fig. 5).

Protein structure, localization, and function

LAMP-2 is a single-spanned transmembrane protein with a molecular mass of 95–120 kDa. The large luminal domain, highly glycosylated through both O- and N-linkages, constitutes about 60 % of the total protein mass and is divided into two homologous parts by a hinge region [11]. The transmembrane domain is followed by a short C-terminal cytoplasmic tail, which has a well-conserved glycine–tyrosine motif, thought to provide a critical signal responsible for LAMP-2 trafficking to lysosomes.

LAMP-2 is mainly localized in the limiting membranes of lysosomes and late endosomes, but is also found in the early endosomal and plasma membranes [6, 11, 12, 20, 26], and amphisome and autolysosome-limiting membranes [7, 34]. In addition, LAMP-2 is also detected in the lumen of lysosomes and endosomes. It has been suggested that the luminal LAMP-2 molecules are soluble, but it is also possible that they are associated with the internal lysosomal/endosomal membranes [6].

LAMP-2 and LAMP-1 (which has high structural similarity to LAMP-2 and is also an abundant lysosomal component) coat the inner surface of the lysosomal membrane and are, therefore, thought to protect the lysosomal membranes and thus the cellular cytoplasmic components from autodigestion by lysosomal proteolytic enzymes. In addition, LAMPs are implicated in the maintenance of the lysosomal acidic environment, and are believed to serve as adhesion molecule when expressed in the plasma membrane.

LAMP-2 is required for the maturation of autophagosomes by fusion with endosomes and lysosomes. LAMP-2 deficiency leads to a failure in the normal process of autophagic maturation: hepatocytes that lack LAMP-2 exhibit accumulation of autophagosomes, but reduction in long-lived protein degradation because of impaired autophagosome function [7, 34]; they also demonstrate intracellular mistargeting of lysosomal enzymes, improper cathepsin D processing, and abnormal retention of mannose-6-phosphate receptors in autophagic vacuoles [7]. These findings suggest that the accumulation of autophagosomes in LAMP-2-deficient hepatocytes (and also in skeletal myofibers) occur because of the defective maturation to autolysosomes, which perform the degradation of the cargo.

In addition, LAMPs are essential for the fusion of lysosomes with phagosomes [17]. Phagosomes deficient in LAMP-1 and LAMP-2 fail to recruit Rab7 necessary for the completion of phagosome maturation [15, 18], and do not fuse with lysosomes.

LAMP-2 also plays a critical role in endosomal cholesterol transport [29]: LAMP-2-deficient animals show cholesterol accumulation in the liver; conversely, LAMP-2 overexpression delays cholesterol accumulation.

Via its cytoplasmic tail, LAMP-2A also performs receptor functions for a selective pathway of cytosolic protein degradation in lysosomes known as chaperone-mediated autophagy (CMA) [2]; LAMP-2A expression in the lysosomal membrane has shown a direct correlation with the activity of the proteolytic pathway [3]. LAMP-2A is highly expressed in the human placenta, lung, liver, kidney, and pancreas, while has low abundance in skeletal muscles [19]. Compared to LAMP-2A, LAMP-2B is more abundantly expressed in the heart, skeletal muscle, and brain at the transcriptional level [19], and the development of Danon disease is largely attributed to LAMP-2B absence [25], as will be discussed later. LAMP-2C acts as a receptor for selective RNA and DNA degradation, termed RNautophagy and DNautophagy, respectively [9, 10].

Animal model of Danon disease

An animal model for Danon disease has been established to determine the molecular mechanisms leading to the phenotypic presentation [28, 34]. LAMP-2-deficient mice have increased mortality: approximately half of them die between 3 and 6 weeks after birth; the surviving population have low body weight, but are fertile and have an almost normal life span. LAMP-2-deficient mice are characterized by hemorrhagic infarction of the small intestine, pancreatic lesions, and altered morphology of the spleen and thymus [34]. Excessive accumulation of autophagosomes in the liver, kidney, pancreas, heart, and skeletal muscle is observed in all knockout mice, including those that survive until reproductive age. Hepatocytes of the LAMP-2-deficient mice have numerous autophagosomal vesicles containing the remains of cell organelles and, sometimes, glycogen; many capillary endothelial cells in the kidney, intestinal wall, lymph nodes, and skeletal and cardiac muscles have autophagic vacuoles, and the majority of neutrophil leukocytes contain large autophagosomes [34]. These findings indicate that LAMP-2-deficient mice have more severe pathologic alterations than patients with Danon disease, which can probably be attributed to the fact that the changes in non-muscular tissues in humans have been overlooked in view of severe cardiac pathology.

Similar to the human disease, LAMP-2-deficient mice display accumulation of autophagosomes in the heart and skeletal muscle where their numbers increase with age [34]. In both LAMP-2-deficient mice and Danon patients, skeletal muscle pathology is more severe in proximal muscles: some vacuoles in these muscle cells contain glycogen and are periodic acid–Schiff staining positive.

The cardiac muscles of Danon-like mice are also functionally impaired, as evidenced by the reduced contraction of their isolated papillary muscles. It has been suggested that, although calcium handling and β-adrenoreceptor response are not altered [31], cardiomyocytes containing large autophagosomal clusters may hamper normal contraction and thus account for a decreased cardiac function.

It should be noted that the accumulation of autophagic vacuoles is not observed in the brain or fibroblasts of LAMP-2-deficient mice. It is possible that the structurally related LAMP-1 might compensate in part for the loss of LAMP-2 in these tissues. This hypothesis is supported by the phenotype of mice deficient in both LAMP-1 and LAMP-2. Whereas single-knockout mice were fertile and viable, the loss of both LAMPs led to embryonic lethality and accumulation of autophagic vacuoles in almost all embryonic tissues [8].

Danon disease and autophagy

Danon disease is caused by the deficiency of lysosomal membrane structural protein, LAMP-2, resulting in the failure of lysosomal biogenesis, maturation, and function.

The view that Danon disease is largely caused by the defects in the LAMP-2B isoform is supported by the fact that the patient containing a mutation in exon 9B, which affects only the LAMP-2B isoform, had a complete set of Danon disease symptoms albeit slightly milder. This notion is further substantiated by the finding that in the heart and skeletal muscle, LAMP-2B was more abundantly expressed at the transcriptional level than LAMP-2A [19]. In this patient, LAMP-2A, which functions as a receptor for chaperone-mediated autophagy (CMA) was likely to have normal expression, suggesting that CMA may not play an essential role in the pathogenic mechanism of Danon disease.

Recently, it has been reported that overexpression of vacuolar protein sorting 34 and 15 (Vps34 and Vps15) protein kinases in the myoblasts of Danon disease patients decreases LC-3 level and alleviates glycogen accumulation [24]. Vps34 and Vps15 kinases are obligate partners acting in complex: Vps 34, a class III phosphatidylinositol 3-kinase (PI3K) converting phosphatidylinositol (PI) to phosphatidylinositol 3-phosphate (PI3P), is essential for protein sorting [30] and Vps15 is a regulatory subunit with putative serine/threonine kinase activity required for Vps34 stability and activation [30]. In mammals, at least three different Vps15/Vps34 complexes regulate different stages of autophagy [23, 35]. The finding that Vps15/Vps34 overexpression in muscle cells derived from Danon patients downregulates LC-3 and glycogen accumulation suggests that the modulation of these protein kinases may lead to a new treatment approach for this lysosomal disorder.

Conclusion

Danon disease is primarily caused by the deficiency of LAMP-2, which plays a role in macroautophagy, CMA, and RNA- and DNA-specific autophagy. Nevertheless, the pathological mechanism of Danon disease is still not fully understood. Further investigation regarding isoform-specific functions is necessary to elucidate the mechanism of Danon disease.

Acknowledgments This study was supported by Intramural Research Grant (26-8) for Neurological and Psychiatric Disorders of NCNP, Comprehensive Research on Disability Health and Welfare from the Ministry of Health, Labor, and Welfare. The authors thank Professor Ikuya Nonaka for his help in electron microscopy analysis, and Ms. Megumu Ogawa and Ms. Kaoru Tatezawa for their technical assistance.

Conflict of interest The authors declare no conflict of interest.

References

1. Boucek D, Jirikowic J, Taylor M (2011) Natural history of Danon disease. Genet Med 13:563–568
2. Cuervo AM, Dice JF (1996) A receptor for the selective uptake and degradation of proteins by lysosomes. Science 273:501–503
3. Cuervo AM, Dice JF (2000) Regulation of lamp2a levels in the lysosomal membrane. Traffic 1:570–583
4. Danon MJ, Oh SJ, DiMauro S et al (1981) Lysosomal glycogen storage disease with normal acid maltase. Neurology 31:51–57
5. Eskelinen EL, Cuervo AM, Taylor MR et al (2005) Unifying nomenclature for the isoforms of the lysosomal membrane protein LAMP-2. Traffic 6:1058–1061
6. Eskelinen EL, Tanaka Y, Saftig P (2003) At the acidic edge: emerging functions for lysosomal membrane proteins. Trends Cell Biol 13:137–145
7. Eskelinen EL, Illert AL, Tanaka Y et al (2002) Role of LAMP-2 in lysosome biogenesis and autophagy. Mol Biol Cell 13:3355–3368
8. Eskelinen EL, Schmidt CK, Neu S et al (2004) Disturbed cholesterol traffic but normal proteolytic function in LAMP-1/LAMP-2 double-deficient fibroblasts. Mol Biol Cell 15:3132–3145
9. Fujiwara Y, Furuta A, Kikuchi H et al (2013) Discovery of a novel type of autophagy targeting RNA. Autophagy 9:403–409
10. Fujiwara Y, Kikuchi H, Aizawa S et al (2013) Direct uptake and degradation of DNA by lysosomes. Autophagy 9:1167–1671
11. Fukuda M (1994) Biogenesis of the lysosomal membrane. Subcell Biochem 22:199–230
12. Furuno K, Ishikawa T, Akasaki K et al (1989) Morphological localization of a major lysosomal membrane glycoprotein in the endocytic membrane system. J Biochem 106:708–716
13. Furuta A, Wakabayashi K, Haratake J et al (2013) Lysosomal storage and advanced senescence in the brain of LAMP-2-deficient Danon disease. Acta Neuropathol 125:459–461
14. Gough NR, Hatem CL, Fambrough DM (1995) The family of LAMP-2 proteins arises by alternative splicing from a single gene: characterization of the avian LAMP-2 gene and identification of mammalian homologs of LAMP-2b and LAMP-2c. DNA Cell Biol 14:863–867
15. Harrison RE, Bucci C, Vieira OV, Schroer TA, Grinstein S (2003) Phagosomes fuse with late endosomes and/or lysosomes by

extension of membrane protrusions along microtubules: role of Rab7 and RILP. Mol Cell Biol 23:6494–6506
16. Hatem CL, Gough NR, Fambrough DM (1995) Multiple mRNAs encode the avian lysosomal membrane protein LAMP-2, resulting in alternative transmembrane and cytoplasmic domains. J Cell Sci 108:2093–2100
17. Huynh KK, Eskelinen EL, Scott CC, Malevanets A, Saftig P, Grinstein S (2007) LAMP proteins are required for fusion of lysosomes with phagosomes. EMBO J 26:313–324
18. Jäger S, Bucci C, Tanida I et al (2004) Role for Rab7 in maturation of late autophagic vacuoles. J Cell Sci 117:4837–4848
19. Konecki DS, Foetisch K, Zimmer KP, Schlotter M, Lichter-Konecki U (1995) An alternatively spliced form of the human lysosome-associated membrane protein-2 gene is expressed in a tissue-specific manner. Biochem Biophys Res Commun 215:757–767
20. Lippincott-Schwartz J, Fambrough DM (1987) Cycling of the integral membrane glycoprotein, LEP100, between plasma membrane and lysosomes: kinetic and morphological analysis. Cell 49:669–677
21. Malicdan MC, Noguchi S, Nonaka I, Saftig P, Nishino I (2008) Lysosomal myopathies: an excessive build-up in autophagosomes is too much to handle. Neuromuscul Disord 18:521–529
22. Malicdan MC, Nishino I (2012) Autophagy in lysosomal myopathies. Brain Pathol 22:82–88
23. Matsunaga K, Saitoh T, Tabata K et al (2009) Two Beclin 1-binding proteins, Atg14L and Rubicon, reciprocally regulate autophagy at different stages. Nat Cell Biol 11:385–396
24. Nemazanyy I, Blaauw B, Paolini C et al (2013) Defects of Vps15 in skeletal muscles lead to autophagic vacuolar myopathy and lysosomal disease. EMBO Mol Med 5:870–890
25. Nishino I, Fu J, Tanji K et al (2000) Primary LAMP-2 deficiency causes X-linked vacuolar cardiomyopathy and myopathy (Danon disease). Nature 406:906–910
26. Nishino I (2006) Autophagic vacuolar myopathy. Semin Pediatr Neurol 13:90–95
27. Nishino I (2003) Autophagic vacuolar myopathies. Curr Neurol and Neurosci Rep 3:64–69
28. Saftig P, Tanaka Y, Lüllmann-Rauch R, von Figura K (2001) Disease model: LAMP-2 enlightens Danon disease. Trends Mol Med 7:37–39
29. Schneede A, Schmidt CK, Hölttä-Vuori M et al (2011) Role for LAMP-2 in endosomal cholesterol transport. J Cell Mol Med 15:280–295
30. Schu PV, Takegawa K, Fry MJ, Stack JH, Waterfield MD, Emr SD (1993) Phosphatidylinositol 3-kinase encoded by yeast VPS34 gene essential for protein sorting. Science 260:88–91
31. Stypmann J, Janssen PM, Prestle J et al (2006) LAMP-2 deficient mice show depressed cardiac contractile function without significant changes in calcium handling. Basic Res Cardiol 101:281–291
32. Sugie K, Yamamoto A, Murayama K et al (2002) Clinicopathological features of genetically confirmed Danon disease. Neurology 58:1773–1778
33. Sugie K, Noguchi S, Kozuka Y et al (2005) Autophagic vacuoles with sarcolemmal features delineate Danon disease and related myopathies. J Neuropathol Exp Neurol 64:513–522
34. Tanaka Y, Guhde G, Suter A et al (2000) Accumulation of autophagic vacuoles and cardiomyopathy in LAMP-2-deficient mice. Nature 406:902–906
35. Zhong Y, Wang QJ, Li X et al (2009) Distinct regulation of autophagic activity by Atg14L and Rubicon associated with Beclin 1-phosphatidylinositol-3-kinase complex. Nat Cell Biol 11:468–476

NEUROPATHOLOGY

Neuropathology 2015; **35**, 91–93 doi:10.1111/neup.12147

Neuropathology Education

Kyphoscoliosis and easy fatigability in a 14-year-old boy

Jantima Tanboon,[1] Yukiko K. Hayashi,[2,3,4] Ichizo Nishino[3,4] and Tumtip Sangruchi[1]

[1]Department of Pathology, Faculty of Medicine, Siriraj Hospital, Mahidol University, Bangkok, Thailand, [2]Department of Neurophysiology, Tokyo Medical University, [3]Department of Neuromuscular Research, National Institute of Neuroscience, and [4]Department of Clinical Development, Translational Medical Center, National Center of Neurology and Psychiatry, Tokyo, Japan

CLINICAL COURSE

The patient was a 14-year-old Thai boy who presented at an orthopedic clinic with kyphoscoliosis first detected 1 year prior to medical attention. He was the first child of non-consanguineous parents; the pregnancy and delivery were uneventful. He had normal developmental milestones. The patient noticed easy fatigability after exercise which worsened during the past year. His younger brother was 10 years old and healthy. There was no history of neuromuscular disease in his family. His father passed away due to an unrelated incident. General examination revealed a body weight of 30 kg and a height of 149 cm, bilateral ptosis, high-arched palate, kyphoscoliosis, and asymmetrical chest wall. Proximal muscle weakness of grade 4 by Medical Research Council Scale in all extremities and areflexia were noted. The muscle tone was normal. Serum CK was 49 IU/L. Echocardiogram showed mild pulmonary and tricuspid regurgitation. Pulmonary function tests showed restrictive lung disease; the forced vital capacity was 1.56 L (51% of predicted). Sleep study revealed apnea-hypopnea index 13.6 per hour associated with severe oxygen desaturation (minimum SpO_2 39.0%).

PATHOLOGICAL FINDINGS

Muscle biopsy from the right quadriceps showed varying fiber sizes with type 1 hypotrophy and type 2 hypertrophy. The type 1 fibers were predominant (91%). Cap structures were seen in 32% of all fibers (Fig. 1). Ultrastructurally, the cap structures were composed of disorganized thin myofibrils and thickened Z-lines (Fig. 2). Nemaline rods were not present. Genetic analysis using genomic DNA identified a heterozygous c.415_417delGAG (p.Glu139del) in exon 4 of *TPM2*. The genetic tests were not performed in other family members.

DIAGNOSIS

TPM2-related cap myopathy.

DISCUSSION

Cap myopathy is a rare congenital myopathy characterized by presence of muscle fibers with cap structures on muscle biopsy and prominent respiratory muscle involvement. It is associated with dominant mutations in *TPM2*, *TPM3* and *ACTA1* genes, in descending order.[1,2]

Histologically, in cases with genetic results, cap structures range from 4% to 100% in muscle fibers.[1] Fidzianska reported two neonatal-onset cases with childhood death containing caps in 70–75% of fibers and two other childhood-onset cases with slowly progressive course containing caps in 20–30% of fibers, suggesting association of disease severity and the frequency of cap structure.[3] The number of caps seems to increase as the patients have aged.[4,5]

Onset of cap myopathy ranges from the neonatal period to childhood. Respiratory insufficiency is usually the major problem in patient management. The other common clinical manifestations include neonatal hypotonia, high-arched palate, myopathic facies and scoliosis. Muscle weakness is predominant in proximal muscles, which is non-specific. Serum CK is usually normal or slightly elevated. A case with distinctive abnormal cardiac function[6] and several cases with mild non-specific cardiac abnormalities have been reported.[1] Interestingly, one of the reported cases shows continuous gradual clinical improvement.[5]

Since all three causative genes in cap myopathy are also associated with nemaline myopathy (NM), it is not surprising to have concurrent caps and rods in the same patients[2,7]

Correspondence: Jantima Tanboon, MD, Department of Pathology, Faculty of Medicine, Siriraj Hospital, Mahidol University, Bangkok Noi, Bangkok 10700, Thailand. Email: jtanboon@gmail.com

Received 14 July 2014 and accepted 20 July 2014; published online 28 August 2014.

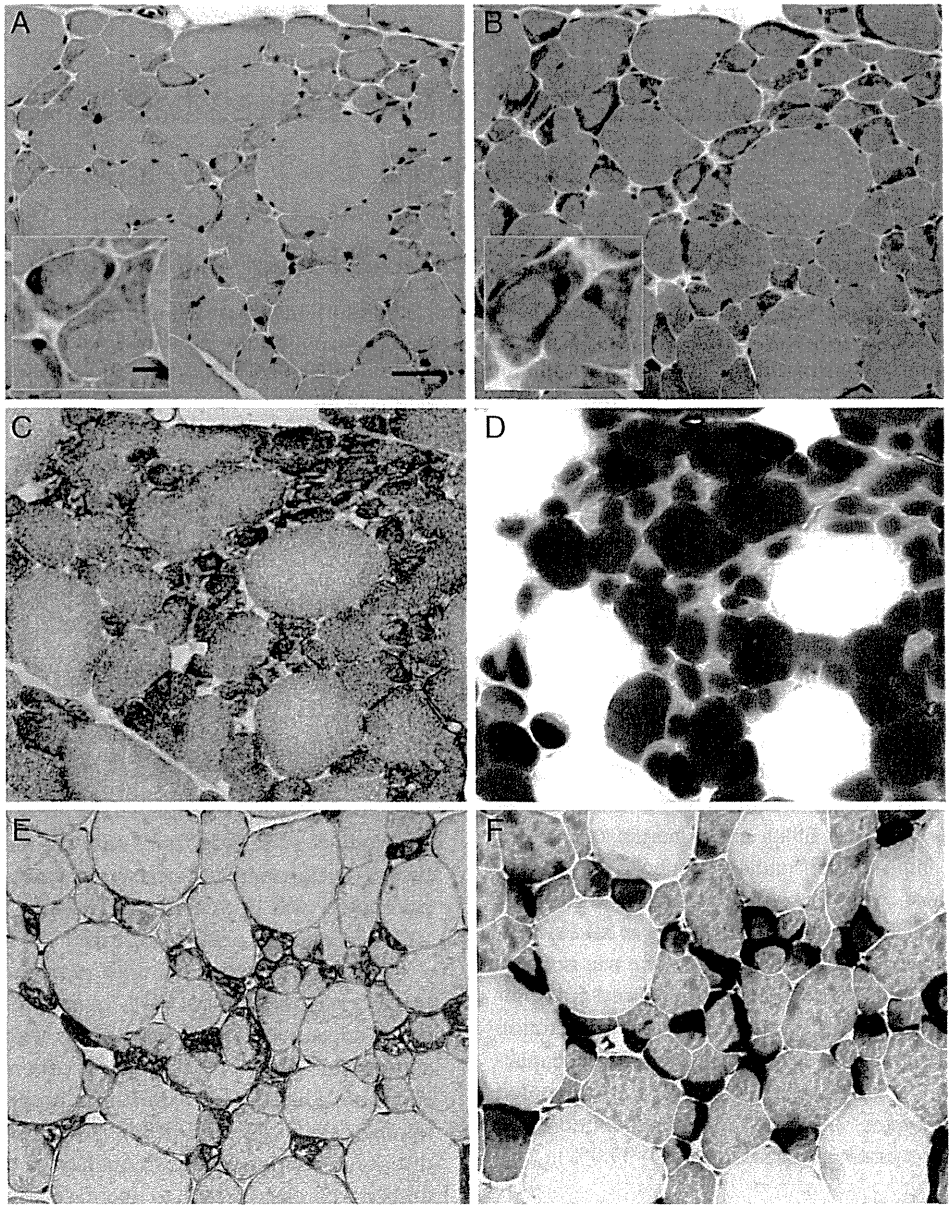

Fig. 1 Cap structures at the periphery of the small fibers in HE stain (A). Caps are highlighted by modified Gomori trichrome stain (B) and nicotinamide adenine dehydrogenase tetrazolium reductase stain (C). The small fibers are type 1 demonstrated by ATPase stain (pH 4.4) and the cap areas are negatively stained (D). The caps are positive for desmin (E) and alpha-actinin (F). Bar = 50 μm, inset bar = 10 μm.

or have a family member with NM[4,8] although cap myopathy is much less common. Muscle biopsy findings of some cap myopathy patients were consistent with congenital fiber type disproportion (CFTD) at a younger age.[5,8] This may represent either a disease spectrum or insufficient tissue sampling since CFTD is also associated with *TPM2* and *TPM3* mutations.[2] Most cap myopathy patients are sporadic yet a few probable autosomal dominant familial cap myopathy cases have been reported.[1,7] It is likely that most cases are affected by *de novo* dominant mutations causing too severe phenotypes to have offspring. Overlapping phenotypes between cap and nemaline myopathies include facial muscle weakness, high-arched palate and respiratory complications. The severity of both myopathies can range from mild to fatal.

The most common recurrent mutation in cap myopathy is p.Glu139del in exon 4 of *TPM2* gene and this mutation seems to be mostly related to cap myopathy, although six patients with different phenotypes have been reported.[2,6,7,9] Most patients with p.Glu139del, including our case, devel-

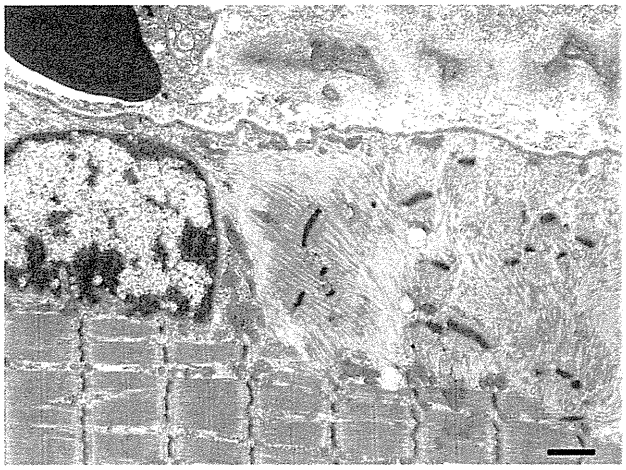

Fig. 2 Electron microscopy study of the cap structures shows disorganized thin myofibrils and thickened Z-lines. Bar = 1 μm.

oped symptoms during childhood, except for one case that presented in the neonatal period.[9] Our patient and two of the reported cases noticed developed scoliosis in a short period of time.[6,7] This feature has not been documented in cap myopathy patients with other mutations. It is possible yet inconclusive that p.Glu139del might affect axial muscles in later stage but progress at a faster rate compared to the other mutations.

In conclusion, we report a case of cap myopathy in a 14-year-old Thai boy. It is the first case reported from Asia and shares a common mutation, p.Glu139del, which was previously identified in patients with European ancestry.[2,6,7,9]

ACKNOWLEDGMENTS

The authors thank Ms. Rangsima Nguenvattana for her secretarial work on the preparation of this manuscript. This work was supported partly by Research on Intractable Diseases, Comprehensive Research on Disability Health and Welfare, and Applying Health Technology from the Ministry of Health Labour and Welfare; partly by Intramural Research Grant 23-5 for Neurological and Psychiatric Disorders of National Center of Neurology and Psychiatry.

DISCLOSURES

All authors report no disclosures.

REFERENCES

1. Schreckenbach T, Schroder JM, Voit T *et al.* Novel TPM3 mutation in a family with cap myopathy and review of the literature. *Neuromuscul Disord* 2014; **24**: 117–124.
2. Marttila M, Lehtokari VL, Marston S *et al.* Mutation update and genotype-phenotype correlations of novel and previously described mutations in TPM2 and TPM3 causing congenital myopathies. *Hum Mutat* 2014; **35**: 779–790.
3. Fidzianska A. "Cap disease" – a failure in the correct muscle fibre formation. *J Neurol Sci* 2002; **201**: 27–31.
4. Cuisset JM, Maurage CA, Pellissier JF *et al.* "Cap myopathy": case report of a family. *Neuromuscul Disord* 2006; **16**: 277–281.
5. Ohlsson M, Quijano-Roy S, Darin N *et al.* New morphologic and genetic findings in cap disease associated with beta-tropomyosin (TPM2) mutations. *Neurology* 2008; **71**: 1896–1901.
6. Clarke NF, Domazetovska A, Waddell L, Kornberg A, McLean C, North KN. Cap disease due to mutation of the beta-tropomyosin gene (TPM2). *Neuromuscul Disord* 2009; **19**: 348–351.
7. Tasca G, Fattori F, Ricci E *et al.* Somatic mosaicism in TPM2-related myopathy with nemaline rods and cap structures. *Acta Neuropathol* 2013; **125**: 169–171.
8. Tajsharghi H, Ohlsson M, Lindberg C, Oldfors A. Congenital myopathy with nemaline rods and cap structures caused by a mutation in the beta-tropomyosin gene (TPM2). *Arch Neurol* 2007; **64**: 1334–1338.
9. Lehtokari VL, Ceuterick-de Groote C, de Jonghe P *et al.* Cap disease caused by heterozygous deletion of the beta-tropomyosin gene TPM2. *Neuromuscul Disord* 2007; **17**: 433–442.

DAG1 mutations associated with asymptomatic hyperCKemia and hypoglycosylation of α-dystroglycan

Mingrui Dong, MD
Satoru Noguchi, PhD
Yukari Endo, MD
Yukiko K. Hayashi, MD, PhD
Shinobu Yoshida, MD, PhD
Ikuya Nonaka, MD, PhD
Ichizo Nishino, MD, PhD

Correspondence to Dr. Noguchi: noguchi@ncnp.go.jp

ABSTRACT

Objectives: To identify gene mutations in patients with dystroglycanopathy and prove pathogenicity of those mutations using an in vitro cell assay.

Methods: We performed whole-exome sequencing on 20 patients, who were previously diagnosed with dystroglycanopathy by immunohistochemistry and/or Western blot analysis. We also evaluated pathogenicity of identified mutations for phenotypic recovery in a *DAG1*-knockout haploid human cell line transfected with mutated DAG1 complementary DNA.

Results: Using exome sequencing, we identified compound heterozygous missense mutations in *DAG1* in a patient with asymptomatic hyperCKemia and pathologically mild muscular dystrophy. Both mutations were in the N-terminal region of α-dystroglycan and affected its glycosylation. Mutated DAG1 complementary DNAs failed to rescue the phenotype in *DAG1*-knockout cells, suggesting that these are pathogenic mutations.

Conclusion: Novel mutations in *DAG1* are associated with asymptomatic hyperCKemia with hypoglycosylation of α-dystroglycan. The combination of exome sequencing and a phenotype-rescue experiment on a gene-knockout haploid cell line represents a powerful tool for evaluation of these pathogenic mutations. ***Neurology*® 2015;84:273–279**

GLOSSARY

cDNA = complementary DNA; ***DAG1*** = dystroglycan 1 (dystrophin-associated glycoprotein 1); **KO** = knockout; **WES** = whole-exome sequencing.

Dystroglycan is a central component of the dystrophin–glycoprotein complex, which links the cytoskeleton and extracellular matrix through sarcolemma.[1,2] Dystroglycan has important roles in the development and maintenance of skeletal muscle, the CNS,[3] and other organs.[4–6] It is encoded by the *DAG1* gene. The synthesized polypeptide is posttranslationally cleaved into 2 subunits, namely, α- and β-dystroglycan; then the former is highly glycosylated.[7,8] α-Dystroglycan is composed of 3 distinct domains: the N-terminal region, the mucin-like domain, and the C-terminal domain, at which the mucin-like domain is highly glycosylated by *O*-linked mannosyl-oligosaccharides and binds to ligands such as laminin and agrin by its sugar chains.[9,10] Reports show that the N-terminal region is required for functional glycosylation of the mucin-like domain by LARGE, an intracellular enzyme-substrate recognition motif necessary for initiation of specific glycosylation.[8,11]

Defects in glycosylation of α-dystroglycan lead to a subgroup of muscular dystrophies and brain and eye malformations, termed dystroglycanopathies.[12] There is a broad spectrum of severity in these diseases, ranging from Walker-Warburg syndrome, muscle-eye-brain disease, and Fukuyama congenital muscular dystrophy to the milder form of limb-girdle muscular dystrophy, such as LGMD2I.[13,14] Recent advances in DNA sequencing techniques facilitated identification of new causative genes in dystroglycanopathies[15–18]; to date, 18 causative genes have been identified. Among them, *DAG1* mutations cause primary dystroglycanopathy in limb-girdle muscular dystrophy[19] and muscle-eye-brain disease.[20]

Supplemental data at Neurology.org

From the Department of Neuromuscular Research, National Institute of Neuroscience (M.D., S.N., Y.E., Y.K.H., I. Nonaka, I. Nishino) and Department of Clinical Development, Translational Medical Center (S.N., Y.E., Y.K.H., I. Nishino), NCNP, Tokyo, Japan; Department of Neurology (M.D.), China-Japan Friendship Hospital, Beijing, China; Department of Neurophysiology (Y.K.H.), Tokyo Medical University; and Department of Pediatrics (S.Y.), Omihachiman Community Medical Center, Shiga, Japan.

Go to Neurology.org for full disclosures. Funding information and disclosures deemed relevant by the authors, if any, are provided at the end of the article.

Herein, we report the case of a patient in whom dystroglycanopathy was caused by novel compound heterozygous missense mutations in *DAG1* identified by whole-exome sequencing (WES) and we prove the pathogenicity of the mutations.

METHODS

Standard protocol approvals, registrations, and patient consents. The ethics committee of the National Center of Neurology and Psychiatry approved this study. All patients gave written informed consent before study participation.

Subjects. To identify the cause of α-dystroglycanopathy, we selected a cohort of 20 unrelated individuals who were diagnosed with α-dystroglycanopathy by negative reactivity with an antibody for glycoepitope of α-dystroglycan (VIA4-1; Millipore, Billerica, MA) on a muscle biopsy and/or decreased VIA4-1 immunoreactivity and laminin binding ability as shown by Western blotting.[21] We immunostained muscle with antibodies for β-dystroglycan (43DAG1; Leica, Wetzlar, Germany), dystrophin (NCL-DYS1, Leica), merosin (4H8-2; Alexis, Lausen, Switzerland), and β-sarcoglycan (5B1, Leica), and conducted Western blotting using the core antibody for α-dystroglycan peptide, GT20ADG. We confirmed that all study patients did not have 3-kb retrotransposal insertion at *FKTN*.

Whole-exome sequencing. WES was performed as reported previously.[22] Briefly, after genomic DNA isolation from muscle specimens or peripheral blood lymphocytes using standard techniques, we performed exon capture according to the manufacturer's instructions (SureSelect Human All Exon kit V4, 50 Mb; Agilent, Santa Clara, CA), followed by paired-end 100-base massively parallel sequencing on an Illumina HiSeq1000 (Illumina, Inc., San Diego, CA). Then, we mapped and aligned to the human genome chromosomal sequence using the Burrows-Wheeler Aligner. We removed duplicate reads using Picard for downstream analysis and conducted local realignments around indels and regions for low base quality scores using the Genome Analysis Toolkit for recalibration. We identified single-nucleotide variants and small indels using the Genome Analysis Toolkit Unified Genotyper (version 1.6) and filtered according to the Broad Institute's best-practice guidelines. We used ANNOVAR to annotate genetic variations. Data filtering included the following conditions: (1) mutation effect—splicing, start lost, exon deletion, frame shift, stop gained or lost, nonsynonymous codon change, codon insertion or deletion; (2) variation frequency less than 0.01 in HapMap and in 1000 Genomes Project database; and (3) inheritance mode—homozygous mutations, hemizygous mutation, or more than 2 mutations in the same genes. We used Sanger sequencing to confirm mutations.

Validation for the pathogenicity of identified mutations. To examine the pathogenicity of identified mutations, we analyzed functional recovery of dystroglycans in *DAG1*-knockout (KO) haploid human cell line (HAP1) cells using transfection of lentivirus vectors, pLVSIN-IRES-ZsGreen (Clontech, Mountain View, CA), harboring wild-type or mutated human DAG1 complementary DNA (cDNA). Jae et al.[23] established the *DAG1*-KO HAP1 cell as reported previously. For the glycosylation in α-dystroglycan assay, we cultured HAP1 cells on laminin-coated glass-bottom dishes. Five days after lentivirus infection, we incubated live cells with IIH6-C4 antibody against glycoepitope of α-dystroglycan (Millipore) in medium and then visualized the cells with Alexa Fluor 568-labeled anti-mouse immunoglobulin M secondary antibody. We observed the cultured cells using a fluorescent microscope (BZ-9000; Keyence, Itasca, IL) with Z-axis scanning throughout whole cells to acquire green fluorescent protein and α-dystroglycan images together (7 images with 1-μm intervals) for full-focus images. After staining with 43DAG1 antibody and GM130 antibody (Cell Signaling Technology, Beverly, MA), we observed localization of β-dystroglycan in formalin-fixed HAP1 cells.

Biotinylation of cell-surface proteins on HAP1 cells. We labeled living HAP1 cells with the membrane-impermeable biotin reagent, Sulfo-NHS-LC-Biotin, according to manufacturer's instructions (Thermo Scientific, Waltham, MA) and then subjected streptavidin-purified proteins to Western blotting using standard techniques. We detected β-dystroglycans with 43DAG1 antibody.

RESULTS

Identification of *DAG1* mutation by WES. After analysis of a cohort of 20 unrelated patients with α-dystroglycanopathy, we identified one patient who harbored mutations in *DAG1* genes. WES analysis summary is presented in table e-1 on the *Neurology*® Web site at Neurology.org. We identified 7 genes with homozygous mutations, 18 genes with compound heterozygous mutations, and 8 genes with hemizygous mutations in this patient (data not shown). Among them, we identified compound heterozygous mutations, c.220G>A (rs189360006) and c.331G>A (rs117209107) in *DAG1*, which are predicted to lead to missense mutations, p.Val74Ile and p.Asp111Asn, respectively. We did not find any other genes involved in the glycosylation pathway in the patient. We confirmed the 2 mutations in *DAG1* by Sanger sequencing (figure 1A) and the compound heterozygosity by transcript analysis (data not shown). Residues at both mutated sites are located in the N-terminal region of α-dystroglycan and are highly conserved during evolution (figure 1, B and C). In silico analyses of mutation function demonstrated that p.Val74Ile and p.Asp111Asn, respectively, were predicted as damaging and tolerated by SIFT and probably damaging and benign in PolyPhen-2, and both mutations were predicted as disease-causing in MutationTaster. Other than *DAG1* mutations, the compound heterozygous missense alterations were found in *TTN* and *AHNAK* genes among muscle-related genes.

Clinical phenotype and histologic features of muscle biopsy. This is a 7-year-old boy coming from a nonconsanguineous marriage who has compound heterozygous mutations in *DAG1*. He was born normally (length at birth, 51.5 cm; birth weight, 3,672 g) and demonstrated normal development milestones. At the age of 4 years and 7 months, he was 98 cm tall, weighed 17 kg, and had a head circumference of 50.8 cm. When he was 4 years

Figure 1 Compound heterozygous mutations in the *DAG1* gene in the described patient

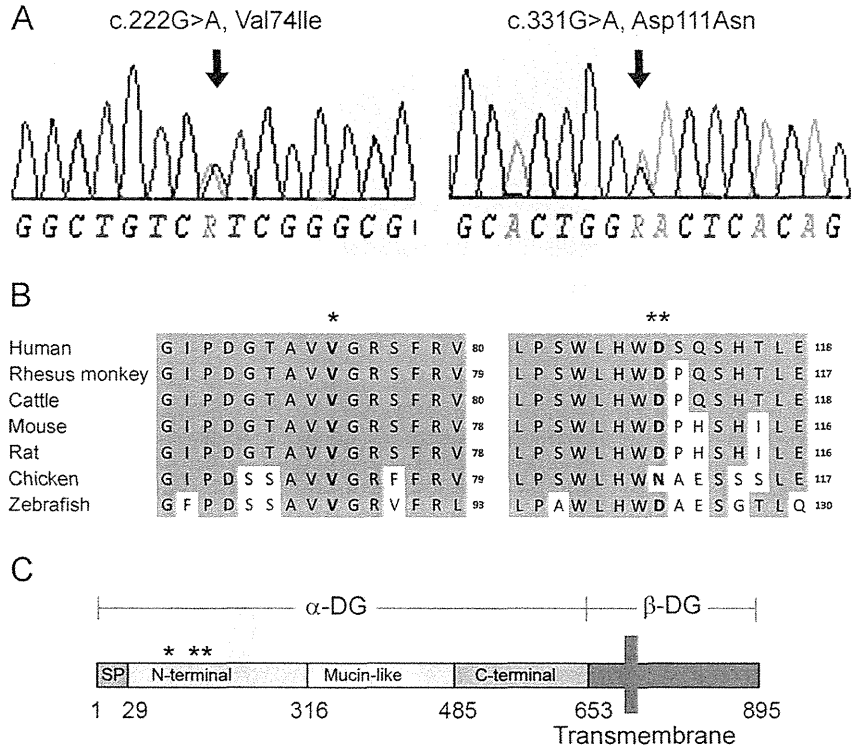

(A) Electropherograms around the mutation sites in *DAG1* genes from Sanger sequencing. (B) Amino acid conservation in mutation sites among species. (C) Localization of mutation sites (* and **) in domain structures in DAG1 protein. DG = dystroglycan.

and 5 months, he became dehydrated in the wake of acute tonsillitis, and was diagnosed with hyperCKemia by chance. After recovery from dehydration, hyperCKemia continued (range, 1,855–6,512 IU/L; normal range, 45–287 IU/L). Physical examination showed no symptomatic muscle weakness but we observed calf pseudohypertrophy. Muscle CT imaging showed low intensity in the rectus femoris, semimembranosus, and gastrocnemius muscles. Brain CT images showed no morphologic abnormality.

Muscle histologic analysis showed muscular dystrophy–like appearance including a few regenerating fibers, internal nuclei, and mild endomysial fibrosis. Immunohistochemical analysis was positive for dystrophin, merosin, sarcoglycans, and β-dystroglycan, but negative for glycoepitope of α-dystroglycan (figure 2). Results of Western blotting and the laminin overlay assay of muscle proteins corroborated the reduction in glycosylation of α-dystroglycan (figure 2); in contrast, we detected strong immunoreactivity to GT20ADG at lower molecular mass. β-Dystroglycan was normal.

Pathogenesis is proven by rescue of *DAG1*-KO HAP1 cells by the wild-type and mutant *DAG1* gene. To prove the pathogenicity of the 2 missense mutations harbored by this patient, we transfected lentivirus vectors with wild-type or mutated DAG1 cDNAs (p.Val74Ile and p.Asp111Asn) into *DAG1*-KO HAP1 cells, which showed defects in reactivity for the anti-α-dystroglycan antibody, IIH6 (figure 3A). *DAG1*-KO HAP1 cells were rescued by introduction of wild-type cDNA showing recovery of strong IIH6 immunoreactivity similar to that of wild-type HAP1 cells (figure 3A). On the contrary, cDNAs with p.Val74Ile and p.Asp111Asn mutations failed to rescue (figure 3A).

We also analyzed mutated β-dystroglycan transport to the cell surface in HAP1 cells. *DAG1*-KO cells were negative for β-dystroglycan staining (figure 3B). Introduction of wild-type and mutated DAG1 cDNAs into *DAG1*-KO cells resulted in recovery of β-dystroglycan staining at the cell surface (in red) but not in the Golgi apparatus (GM130, blue), suggesting that processing and transport of dystroglycan was not affected by the mutations. Cell-surface biotin-labeling experiments in *DAG1*-KO cells transfected with wild-type and mutated DAG1 cDNAs also showed recovery of β-dystroglycan in the biotinylated protein fraction (figure 3C). These results demonstrate that these 2 mutations are pathogenic and impair glycosylation of α-dystroglycan, but not dystroglycan expression.

Figure 2 Hypoglycosylation of α-dystroglycan in the described patient

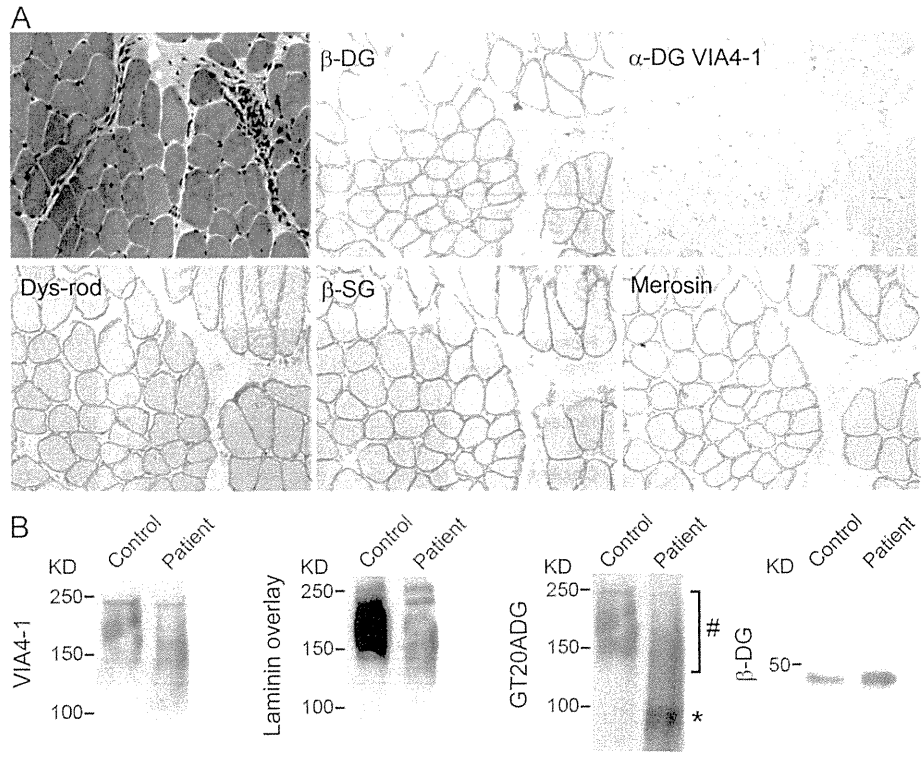

(A, top) Histology and immunostaining of skeletal muscle from the patient. Muscle histology showed muscular dystrophy-like appearance including a few regenerating fibers, internal nuclei, and mild endomysial fibrosis. (A, bottom) Muscle stained positive for antibodies to dystrophin (Dys-rod), merosin, β-sarcoglycan (β-SG), and β-dystroglycan (β-DG), but negative for glycoepitope antibody to α-dystroglycan (α-DG VIA4-1). (B) Western blotting with VIA4-1 antibody and the laminin overlay assay of muscle proteins showing reduced glycosylation of α-dystroglycan; in contrast, strong immunoreactivity to GT20ADG for core peptide was detected at lower molecular mass (*). After Western blotting with VIA4-1 antibody, the same membrane was used for GT20ADG. The bands labeled with # were the VIA4-1 antibody-reactive bands. β-Dystroglycan staining was normal.

DISCUSSION Herein, we report on a patient with dystroglycanopathy, who has compound heterozygous mutations in *DAG1*. This patient had asymptomatic hyperCKemia with mild muscular dystrophy and deficiency in laminin-binding glycosylation in α-dystroglycan. Although the patient could be presymptomatic for muscle weakness or intellectual disability, the clinical phenotype is much milder compared with a previous report of a patient who had limb-girdle–type muscular dystrophy accompanied by mild cognitive impairment.[19] Our finding expands the clinical and pathologic spectrum of dystroglycanopathy associated with *DAG1* mutation from a muscle-eye-brain disease–like phenotype and mild limb-girdle muscular dystrophy[19,20] to asymptomatic hyperCKemia. Myopathic asymptomatic hyperCKemia has been reported in secondary dystroglycanopathies, with mutations in *FKRP* and *FKTN* genes.[24–26] By WES, we also identified 2 missense alterations in each of the *TTN* and *AHNAK* genes, which have been known to be expressed in skeletal muscles. Both alterations in *TTN* were predicted as probably damaging in PolyPhen-2 or disease-causing in MutationTaster in silico functional analyses. These alterations in *TTN* were not localized in the exons in which the mutations have been identified in other muscle diseases, such as hereditary myopathy with early respiratory failure, cardiomyopathy, or tibial muscular dystrophy. *AHNAK* missense alterations were predicted as probably damaging and benign in PolyPhen-2 or polymorphism in MutationTaster. Functional experiments for the mutated proteins would be required for final conclusion of their pathogenicities.

Although one could argue whether the c.220G>A and c.331G>A variants previously annotated in the dbSNP131, 1000 Genomes, and HapMap databases can be the candidate pathogenic mutations, we still presume they are pathogenic because we did not find any other strong candidate gene for dystroglycanopathy in this patient. Because it is known that the 3-kb retrotransposal insertion in *FKTN* with a frequency of 1/88 allele is associated with a high prevalence of Fukuyama congenital muscular dystrophy in Japan,[27]

Figure 3 Mutant *DAG1* observed in patients does not rescue hypoglycosylation of α-dystroglycan in *DAG1*-KO cells

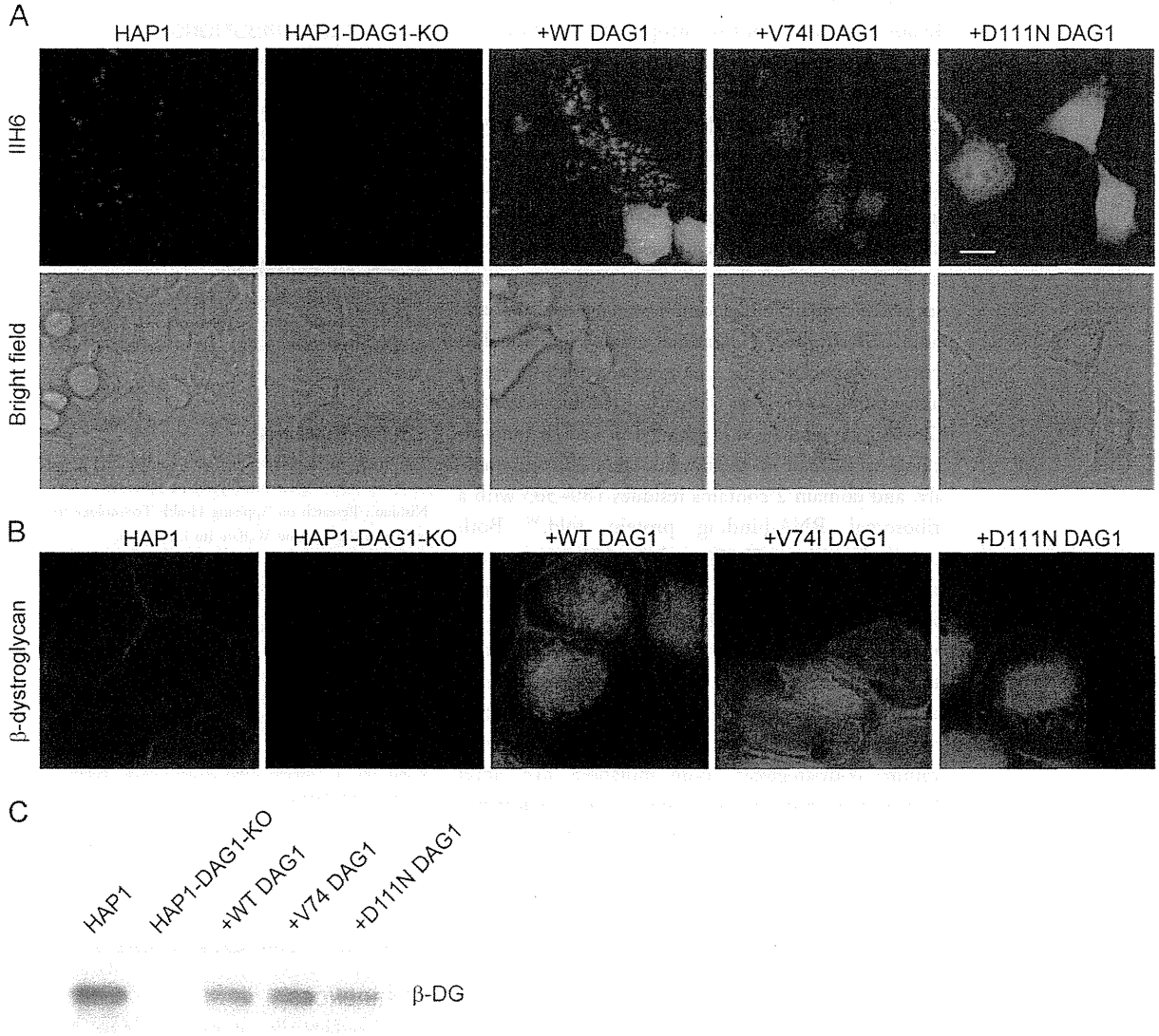

(A) IIH6-4C2 staining of wild-type HAP1 cells (in red), DAG1-knockout cells (HAP1-DAG1-KO), and DAG1-KO cells transfected with wild-type (+WT-DAG1), Val74Ile-mutated (+V74I DAG1), and Asp111Asn-mutated DAG1 (+D111N DAG1). Transfected cells are positive for ZsGreen expression (in green). (B, C) Recovery of β-dystroglycan on cell surface in DAG1-KO cells by transfection with wild-type (+WT-DAG1), p.Val74Ile-mutated (+V74I DAG1), and p.Asp111Asn-mutated DAG1 (+D111N DAG1). HAP1, wild-type haploid cells; HAP1-DAG1-KO, DAG1-KO HAP1 cells. (B) Immunostaining of β-dystroglycan (red) and Golgi protein, GM130 (blue). (C) Western blot analysis of cell-surface biotin-labeled fraction. Scale bar denotes 20 μm. β-DG = β-dystroglycan.

it is logical to suspect a mutation with a variation frequency of more than 0.01. Because the c.331G>A mutation has a variation frequency of 0.005 in all populations in 1000 Genomes and a higher frequency (0.028) in the Japanese population in the Human Genetic Variation Database, there is a possibility that a higher incidence of potential dystroglycanopathy caused by p.Asp111Asn substitution exists in the Japanese population. However, in other populations, the frequency has not been known.

As reported, hypoglycosylation levels of α-dystroglycan do not consistently correlate with clinical severity.[28] Our patient should be classified as having a primary dystroglycanopathy with mutations in *DAG1*; he had typical hypoglycosylation of α-dystroglycan in terms of low molecular mass of the protein, positive reactivity to anti-core peptide antibody, and decreased binding to laminin, but he showed a milder phenotype. The level of hypoglycosylation of α-dystroglycan is not necessarily predictive of phenotypic severity in dystroglycanopathy.

Our results suggest that the missense mutation of p.Val74Ile or p.Asp111Asn in the N-terminal region of α-dystroglycan does not influence expression of the dystroglycan, but it does cause a defect in

posttranslational modification. Similarly, Hara et al.[19] reported a missense mutation (p.The192Met) in the N-terminal region, which is also associated with hypoglycosylation of α-dystroglycan but with normal β-dystroglycan localization. LARGE catalyzes the extension of specific disaccharide structures [−3GlcAα1−4Xylβ1−] on a phosphorylated *O*-mannosyl glycan in the mucin-like domain, which is required for laminin binding, within the Golgi apparatus.[29] The N-terminal region in α-dystroglycan serves as a recognition site for LARGE[8]; of note, Hara et al. demonstrated that the p.The192Met mutation in *DAG1* impairs interaction between α-dystroglycan and LARGE. This N-terminal region is predicted to have L-shaped modular architecture and comprises 2 autonomous domains; domain 1 contains residues 28–168 in murine α-dystroglycan and belongs to the I-set domain of the immunoglobulin superfamily, and domain 2 contains residues 180–303 with a ribosomal RNA-binding protein fold.[30] Both mutated residues, Val74 and Asp111, are present in domain 1 and are neighbors of Gly75 and Gln113 (corresponding to Gly73 and His111in murine dystroglycan); each of these is predicted to be aligned on the interaction between domain 1 and 2, and the trimer interface of domain 1, respectively, in the crystal structure of the N-terminal region of murine α-dystroglycan. Both mutations may affect higher-order structural formation of the N-terminal region of α-dystroglycan. Another possibility is that the mutations may impair direct interaction of the N-terminal globular region of α-dystroglycan with extracellular matrix molecules, as suggested by Hall et al.[31] Remarkable secondary structure and hydrophobic character changes of the mutated fragment are reported to lead to weaker interaction of this domain with laminin.[32]

Previously, Willer et al.[15] have demonstrated the rescuing experiments using patients' fibroblasts in dystroglycanopathy for evaluation of the pathogenicity of gene mutations. In this study, we used gene-modified HAP1 cells because the patient's cells were not available. The phenotypic rescue experiments described here, using *DAG1*-KO HAP1 cells with lentivirus-mediated expression of mutated cDNA, enabled rapid and easy evaluation of the pathogenicity of the mutations. This is a simple method based on the recovery of the function of α-dystroglycan. Theoretically, this method can be applied to evaluate any of the mutations in all known causative genes as well as mutations in novel candidate genes for dystroglycanopathies without requiring enzymatic activity measurement, as long as the specific gene-KO HAP1 cells are available. This method would be applicable by any researcher for confirming the data from WES for each causative mutation in any disease, if the phenotypes of cells were characterized.

AUTHOR CONTRIBUTIONS

M.D. conducted acquisition, analysis and interpretation of data, and drafted and edited the manuscript. S.N. supervised all aspects of this study including study design, data interpretation, and drafted and edited the manuscript. Y.E. made WES pipeline and analyzed the data. Y.K.H. selected patients and performed WES. S.Y. collected clinical information of the patient. I. Nonaka and I. Nishino supervised manuscript preparation and edited the manuscript.

ACKNOWLEDGMENT

The authors thank Nozomi Matsuyama, Megumu Ogawa, Kanako Goto, and Asako Kaminaga for technical support, Thijn R. Brummelkamp for supplying HAP1 cells, and Kevin P. Campbell for supplying GT20ADG antibody.

STUDY FUNDING

This study was partially supported by Intramural Research Grant (25-5, 26-8) for Neurological and Psychiatric Disorders of NCNP (to S.N., I. Nishino); Research on Applying Health Technology from the Ministry of Health, Labour and Welfare (to I. Nishino).

DISCLOSURE

M. Dong reports no disclosures relevant to the manuscript. S. Noguchi serves as an editor of *Acta Neuropathologica Communications* and received research support from the Ministry of Health, Labour and Welfare. Y. Endo reports no disclosures relevant to the manuscript. Y. Hayashi received research support from the Ministry of Health, Labour and Welfare. S. Yoshida and I. Nonaka report no disclosures relevant to the manuscript. I. Nishino serves as an associate editor of *Neuromuscular Disorders* and *Neurology and Clinical Neuroscience*, serves on the speakers bureau of Genzyme and Kitano Hospital, serves as a consultant of Novartis Pharma, and received research support from Genzyme and the Ministry of Health, Labour and Welfare. Go to Neurology.org for full disclosures.

Received May 31, 2014. Accepted in final form September 29, 2014.

REFERENCES

1. Ibraghimov-Beskrovnaya O, Ervasti JM, Leveille CJ, Slaughter CA, Sernett SW, Campbell KP. Primary structure of dystrophin-associated glycoproteins linking dystrophin to the extracellular matrix. Nature 1992;355:696–702.
2. Michele DE, Barresi R, Kanagawa M, et al. Post-translational disruption of dystroglycan-ligand interactions in congenital muscular dystrophies. Nature 2002;418:417–422.
3. Moore SA, Saito F, Chen J, et al. Deletion of brain dystroglycan recapitulates aspects of congenital muscular dystrophy. Nature 2002;418:422–425.
4. Saito F, Moore SA, Barresi R, et al. Unique role of dystroglycan in peripheral nerve myelination, nodal structure, and sodium channel stabilization. Neuron 2003;38:747–758.
5. Durbeej M, Talts JF, Henry MD, Yurchenco PD, Campbell KP, Ekblom P. Dystroglycan binding to laminin alpha1LG4 module influences epithelial morphogenesis of salivary gland and lung in vitro. Differentiation 2001;69:121–134.
6. Matsumura K, Chiba A, Yamada H, et al. A role of dystroglycan in schwannoma cell adhesion to laminin. J Biol Chem 1997;272:13904–13910.

7. Noguchi S, Wakabayashi E, Imamura M, Yoshida M, Ozawa E. Formation of sarcoglycan complex with differentiation in cultured myocyte. Eur J Biochem 2000;267: 640–648.
8. Kanagawa M, Saito F, Kunz S, et al. Molecular recognition by LARGE is essential for expression of functional dystroglycan. Cell 2004;117:953–964.
9. Brancaccio A, Schulthess T, Gesemann M, Engel J. Electron microscopic evidence for a mucin-like region in chick muscle alpha-dystroglycan. FEBS Lett 1995;368: 139–142.
10. Chiba A, Matsumura K, Yamada H, et al. Structures of sialylated O-linked oligosaccharides of bovine peripheral nerve alpha-dystroglycan: the role of a novel O-mannosyl-type oligosaccharide in the binding of alpha-dystroglycan with laminin. J Biol Chem 1997; 272:2156–2162.
11. Hara Y, Kanagawa M, Kunz S, et al. Like-acetylglucosaminyltransferase (LARGE)-dependent modification of dystroglycan at Thr-317/319 is required for laminin binding and arenavirus infection. Proc Natl Acad Sci USA 2011;108:17426–17431.
12. Muntoni F, Brockington M, Brown SC. Glycosylation eases muscular dystrophy. Nat Med 2004;10:676–677.
13. Brown SC, Torelli S, Brockington M. Abnormalities in alpha-dystroglycan expression in MDC1C and LGMD2I muscular dystrophies. Am J Pathol 2004;164:727–737.
14. Mendell JR, Boué DR, Martin PT. The congenital muscular dystrophies: recent advances and molecular insights. Pediatr Dev Pathol 2006;9:427–443.
15. Willer T, Lee H, Lommel M, et al. ISPD loss-of-function mutations disrupt dystroglycan O-mannosylation and cause Walker-Warburg syndrome. Nat Genet 2012;44: 575–580.
16. Roscioli T, Kamsteeg EJ, Buysse K, et al. Mutations in ISPD cause Walker-Warburg syndrome and defective glycosylation of α-dystroglycan. Nat Genet 2012;44: 581–585.
17. Manzini MC, Tambunan DE, Hill RS, et al. Exome sequencing and functional validation in zebrafish identify GTDC2 mutations as a cause of Walker-Warburg syndrome. Am J Hum Genet 2012;91:541–547.
18. Carss KJ, Stevens E, Foley AR, et al. Mutations in GDP-mannose pyrophosphorylase B cause congenital and limb-girdle muscular dystrophies associated with hypoglycosylation of α-dystroglycan. Am J Hum Genet 2013; 93:29–41.
19. Hara Y, Balci-Hayta B, Yoshida-Moriguchi T, et al. A dystroglycan mutation associated with limb-girdle muscular dystrophy. N Engl J Med 2011;364:939–946.
20. Geis T, Marquard K, Rödl T. Homozygous dystroglycan mutation associated with a novel muscle-eye-brain disease-like phenotype with multicystic leucodystrophy. Neurogenetics 2013;14:205–213.
21. Hayashi YK, Ogawa M, Tagawa K, et al. Selective deficiency of alpha-dystroglycan in Fukuyama-type congenital muscular dystrophy. Neurology 2001;57:115–121.
22. Saitsu H, Nishimura T, Muramatsu K, et al. De novo mutations in the autophagy gene WDR45 cause static encephalopathy of childhood with neurodegeneration in adulthood. Nat Genet 2013;45:445–449.
23. Jae LT, Raaben M, Riemersma M, et al. Deciphering the glycosylome of dystroglycanopathies using haploid screens for lassa virus entry. Science 2013;340:479–483.
24. de Paula F, Vieira N, Starling A, et al. Asymptomatic carriers for homozygous novel mutations in the FKRP gene: the other end of the spectrum. Eur J Hum Genet 2003;11:923–930.
25. Fernandez C, de Paula AM, Figarella-Branger D, et al. Diagnostic evaluation of clinically normal subjects with chronic hyperCKemia. Neurology 2006;66:1585–1587.
26. Fiorillo C, Moro F, Astrea G, et al. Novel mutations in the fukutin gene in a boy with asymptomatic hyperCKemia. Neuromuscul Disord 2013;23:1010–1015.
27. Colombo R, Bignamini AA, Carobene A, et al. Age and origin of the FCMD 3'-untranslated-region retrotransposal insertion mutation causing Fukuyama-type congenital muscular dystrophy in the Japanese population. Hum Genet 2000;107:559–567.
28. Jimenez-Mallebrera C, Torelli S, Feng L, et al. A comparative study of alpha-dystroglycan glycosylation in dystroglycanopathies suggests that the hypoglycosylation of alpha-dystroglycan does not consistently correlate with clinical severity. Brain Pathol 2009;19:596–611.
29. Yoshida-Moriguchi T, Yu L, Stalnaker SH, et al. O-mannosyl phosphorylation of alpha-dystroglycan is required for laminin binding. Science 2010;327:88–92.
30. Bozic D, Sciandra F, Lamba D, Brancaccio A. The structure of the N-terminal region of murine skeletal muscle alpha-dystroglycan discloses a modular architecture. J Biol Chem 2004;279:44812–44816.
31. Hall H, Bozic D, Michel K, Hubbell JA. N-terminal alpha-dystroglycan binds to different extracellular matrix molecules expressed in regenerating peripheral nerves in a protein-mediated manner and promotes neurite extension of PC12 cells. Mol Cell Neurosci 2003;24:1062–1073.
32. Bhattacharya S, Das A, Ghosh S, Dasgupta R, Bagchi A. Hypoglycosylation of dystroglycan due to T192M mutation: a molecular insight behind the fact. Gene 2014;537: 108–114.

doi:10.1093/brain/awu210 Brain 2014: 137; 2670–2679 | 2670

BRAIN
A JOURNAL OF NEUROLOGY

Sialyllactose ameliorates myopathic phenotypes in symptomatic GNE myopathy model mice

Takahiro Yonekawa,[1,2] May Christine V. Malicdan,[3] Anna Cho,[1] Yukiko K. Hayashi,[1,4,5] Ikuya Nonaka,[1] Toshiki Mine,[6] Takeshi Yamamoto,[6] Ichizo Nishino[1,2,4] and Satoru Noguchi[1,4]

1 Department of Neuromuscular Research, National Institute of Neuroscience, National Centre of Neurology and Psychiatry (NCNP), Tokyo, Japan
2 Department of Education, Interdisciplinary Graduate School of Medicine and Engineering, University of Yamanashi, Yamanashi, Japan
3 Medical Genetics Branch, National Human Genome Research Institute, National Institutes of Health, Bethesda, MD, USA
4 Department of Clinical Development, Translational Medical Centre, NCNP, Tokyo, Japan
5 Department of Neurophysiology, Tokyo Medical University, Tokyo, Japan
6 Glycotechnology Business Unit, Japan Tabacco Inc, Shizuoka, Japan

Correspondence to: Satoru Noguchi, Ph.D.,
Department of Neuromuscular Research, National Institute of Neuroscience, NCNP, 4-1-1,
Ogawa-Higashicho, Kodaira, Tokyo 1878502, Japan
E-mail: noguchi@ncnp.go.jp

Patients with GNE myopathy, a progressive and debilitating disease caused by a genetic defect in sialic acid biosynthesis, rely on supportive care and eventually become wheelchair-bound. To elucidate whether GNE myopathy is treatable at a progressive stage of the disease, we examined the efficacy of sialic acid supplementation on symptomatic old GNE myopathy mice that have ongoing, active muscle degeneration. We examined the therapeutic effect of a less metabolized sialic acid compound (6′-sialyllactose) or free sialic acid (*N*-acetylneuraminic acid) by oral, continuous administration to 50-week-old GNE myopathy mice for 30 weeks. To evaluate effects on their motor performance in living mice, spontaneous locomotion activity on a running wheel was measured chronologically at 50, 65, 72 and 80 weeks of age. The size, force production, and pathology of isolated gastrocnemius muscle were analysed at the end point. Sialic acid level in skeletal muscle was also measured. Spontaneous locomotion activity was recovered in 6′-sialyllactose-treated mice, while NeuAc-treated mice slowed the disease progression. Treatment with 6′-sialyllactose led to marked restoration of hyposialylation in muscle and consequently to robust improvement in the muscle size, contractile parameters, and pathology as compared to NeuAc. This is due to the fact that 6′-sialyllactose is longer working as it is further metabolized to free sialic acid after initial absorption. 6′-sialyllactose ameliorated muscle atrophy and degeneration in symptomatic GNE myopathy mice. Our results provide evidence that GNE myopathy can be treated even at a progressive stage and 6′-sialyllactose has more remarkable advantage than free sialic acid, providing a conceptual proof for clinical use in patients.

Keywords: amyloid inclusion; distal myopathy with rimmed vacuoles (DMRV)/hereditary inclusion body myopathy (hIBM); GNE myopathy; hyposialylation; sialyllactose

Abbreviations: CSA = cross-sectional area; ManNAc = *N*-acetylmannosamine; NeuAc = *N*-acetylneuraminic acid

Introduction

GNE myopathy, also called distal myopathy with rimmed vacuoles or hereditary inclusion body myopathy, is an adult-onset, moderately progressive autosomal recessive myopathy. The disease is characterized clinically by initial atrophy of the tibialis anterior and hamstring muscles and relative sparing of the quadriceps femoris muscle, and pathologically by rimmed vacuoles and

Received April 18, 2014. Revised June 25, 2014. Accepted June 26, 2014. Advance Access publication July 24, 2014

intracellular accumulation of amyloid and other proteins (Nishino *et al.*, 2002; Nonaka *et al.*, 2005). GNE myopathy is due to mutations in the *GNE* gene that encodes a bifunctional enzyme, uridine diphospho-*N*-acetylglucosamine 2-epimerase and *N*-acetylmannosamine (ManNAc) kinase (Eisenberg *et al.*, 2001; Nishino *et al.*, 2002), which catalyses the critical two steps in sialic acid biosynthesis. Mutations in the *GNE* gene lead to significant reduction in either or both of the two enzymatic activities of the gene product (Hinderlich *et al.*, 2004; Noguchi *et al.*, 2004), and lead to reduced sialic acid levels in the serum, skeletal muscle, and cultured cells from patients with GNE myopathy (Noguchi *et al.*, 2004). These findings were further supported by observations in the model mouse ($Gne^{-/-}$ with human *GNE* Asp176Val-transgenic mouse) that recapitulates the myopathic features in human patients and shows hyposialylation in the serum and other tissues from birth and manifested progressive muscle weakness and atrophy from 21 weeks of age, followed by intracytoplasmic inclusions (~31 weeks) and rimmed vacuole formation (~41 weeks) (Malicdan *et al.*, 2007).

To date, patients with GNE myopathy rely on supportive care of symptoms and eventually become wheelchair-bound within ~12 years after onset (Nishino *et al.*, 2002; Nonaka *et al.*, 2005). We have shown the prophylactic effect of sialic acid-related natural compounds, i.e. *N*-acetylneuraminic acid (NeuAc, free sialic acid), NeuAc's glycosyl conjugate, 6'-sialyllactose, and NeuAc's biosynthetic precursor, ManNAc, in GNE myopathy mice (Malicdan *et al.*, 2009). This study provided basis for clinical trials for patients with GNE myopathy that are currently ongoing, using ManNAc and NeuAc (ClinicalTrials.gov, 2014) but had limitations. As this study was designed to prove prophylactic effect of sialic acid supplementation on the development of myopathy, it is necessary to examine whether myopathic symptoms can actually be recovered by sialic acid treatment once they appear. Given that physicians usually see affected individuals who have already developed muscle atrophy and degeneration, the proof that muscle size and strength are restored in patients at clinical stage is of practical importance. Taking on this endeavor is not without caveat, as preclinical trials using aged, symptomatic mice for a prolonged period of time raise several issues. First, we needed outcome measures to assess the motor performance even in affected mice manifesting severe muscle weakness. Overloaded motor exercise may not be ideal because it may worsen the morbidity or influence the mortality of affected mice. GNE myopathy mice show <50% survival rate and severely worsened motor activity at 50 weeks of age (Malicdan *et al.*, 2007), thus a method that is not physically stressful and one that can be repeated should be considered. Second, there are difficulties with interpreting the results of *in vivo* experiments using a heterogeneous group of myopathic mice due to some variability in the onset of muscle degeneration, requiring baseline chronological measurement during intended age and period of treatment. In this study, we attempted to evaluate the effect of sialic acid supplementation on myopathic phenotype in the symptomatic GNE myopathy mouse model using an assessment system that might be widely adaptable to studies using other symptomatic mouse models.

Furthermore, the pharmacological properties and cellular incorporation efficiency of sialic acid compounds should be considered. We have recently reported that peracetylated ManNAc was markedly incorporated into human GNE myopathy cells (Malicdan *et al.*, 2012). Peracetylated ManNAc, a synthetic compound, prevented the development of myopathic phenotype in the GNE myopathy mice in a dose-dependent manner but also raised cellular sialic acid levels in various tissues beyond normal levels, raising concerns about hypersialylation, even though it was rapidly excreted into urine like other sialic acid compounds. On the other hand, less metabolized compounds are supposed to circulate through the body for a longer time to give an opportunity to peripheral tissues to incorporate these compounds. In our previous preclinical studies, even with one-third of sialic acid amounts in 6'-sialyllactose in molar ratio, it provided a similar prophylactic effect as free NeuAc and ManNAc in preventing the development of myopathic phenotype in the GNE myopathy mice (Malicdan *et al.*, 2009). When given orally, 6'-sialyllactose has been reported to have a longer retention in blood than NeuAc (Nöule and Schauer, 1981). In this study, we evaluated the effects of a sustained compound, 6'-sialyllactose, in the recovery of cellular sialylation and myopathic phenotype in symptomatic old GNE myopathy mice.

Materials and methods

The GNE myopathy mice were generated as reported previously (Malicdan *et al.*, 2007). Mice were maintained in a barrier-free, specific pathogen-free grade facility on a 12-h light, 12-h dark cycle and had free access to normal chow and water. All animal experiments conducted in this study were approved by and carried out within the rules and regulations of the Ethical Review Committee on the Care and Use of Rodents in the National Institute of Neuroscience, National Centre of Neurology and Psychiatry (NCNP). These policies are based on the 'Guideline for Animal Experimentation' as sanctioned by the Council of the Japanese Association of Laboratory Animal Science.

NeuAc was purchased from Japan Food and Liquor Alliance, and ManNAc was purchased from Sigma-Aldrich. 6'-sialyllactose was produced with genetically engineered *Escherichia coli* expressing α2,6-sialyltransferase gene from *Photobacterium* sp. JT-ISH-224 and CMP-NeuAc synthase gene from *Neisseria meningitides* and purified according to the methods reported by Drouillard *et al.* (2010). The purity and structure was confirmed by HPLC (Endo *et al.*, 2009) and ^{1}H-NMR spectrum, respectively.

Cultured myoblasts from a patient with GNE myopathy carrying homozygous Asp176Val mutations in the *GNE* gene were obtained with informed consent approved by the Ethical Review Board at the NCNP. Myoblasts were cultured in 10% foetal bovine serum, Dulbecco's modified Eagle medium (DMEM)/F-12 (Sigma-Aldrich) in a humidified chamber with 5% CO_2 at 37°C. Myogenic differentiation was induced at confluence stage by switching the medium to 5% horse serum in DMEM/F-12. Seventy-two hours before sialic acid determination, the medium was replaced with serum-free DMEM/F-12 with or without NeuAc, ManNAc and 6'-sialyllactose and maintained in the humidified chamber for 72 h. Sialic acids were hydrolyzed in 25 mM sulphuric acid for 1 h at 80°C. Released sialic acids were then derivatized with 1,2-diamino-4,5-methylenedioxybenzene and analysed with reversed-phase HPLC as described previously (Hara *et al.*, 1989; Malicdan *et al.*, 2007). Total proteins in tissues and cultured cells were measured using Pierce BCA kit according to the manufacturer's protocol.

For the experiment of 6'-sialyllactose pharmacokinetics, three wild-type mice were used. After collection of blood from the tail vein and urine for baseline data before administration, 30 mg of 6'-sialyllactose was given via an intragastric route. The urine and blood were then serially collected after 5, 10, 30, 60, 120, 240 and 480 min. At the end of the experiment, the mice were sacrificed. The urine and prepared plasma were frozen and kept at −20°C until processing. To quantify 6'-sialyllactose, samples were labelled with 4-aminobenzoic acid ethyl ester according to the manufacturer's protocol (ABEE Labelling Kit, J-Oilmills). Fluorescence labelled mono- and disaccharides, and 6'-sialyllactose were chromatographed on an amide-80 in 80% acetonitrile in 0.5 M acetic acid/triethylamine (pH 7.3) at a flow rate of 1.0 ml/min for analysis. Total sialic acids from those prepared plasmas were also measured.

For oral 6'-sialyllactose or NeuAc treatment, GNE myopathy mice, including corresponding littermates, whose ages were ~50 weeks, were included in the cohort. The GNE myopathy mice were divided into four groups: non-treated ($n = 18$) given acid water, low dose ($n = 10$) given 6'-sialyllactose at 100 mg/kg/d, high dose ($n = 8$) given 6'-sialyllactose at 1000 mg/kg/d, and NeuAc ($n = 11$) given at 1000 mg/kg/d. 6'-sialyllactose and NeuAc, computed according to the desired dose per day, were mixed with the drinking water and given continuously until the mice reached 80 weeks of age. A few control littermates (*Gne*$^{+/-}$ or *Gne*$^{+/-}$ *hGNE* Asp176Val-Tg) per group were also treated for toxicological examination.

Voluntary exercise within an individual mouse cage was repeatedly measured. A running wheel (SW-15, MELQUEST) was fixed up into a rearing cage to measure spontaneous locomotor activity. The output signal of 1 pulse per revolution by an on/off signal of microswitch was saved to a PC with software for data collection (CIF3Win, Neuroscience). Voluntary exercise was quantified as the total number of wheel revolutions in 72 h. The data were serially collected for mice at 50, 65, 72 and 80 weeks of age. Because of a marked variation among GNE myopathy mice at 50 weeks of age, we used the relative values at 65, 72 and 80 weeks to the initial measurement at 50 weeks for each mouse.

In a preliminary NeuAc treatment study, the motor performance was evaluated using treadmill exercise as previously reported (Malicdan *et al.*, 2008). After 7 days of acclimation on the treadmill, the performance tests were carried out three times, on separate days. The test began with a speed of 20 m/min, which was increased by 10 m/min every minute until the tested mouse was exhausted and could no longer run. The time of exhaustion was used to calculate the distance that the mouse covered during the exercise.

Measurement of the contractile properties of gastrocnemius and tibialis anterior muscles was performed according to previous report (Malicdan *et al.*, 2008). All materials used for *in vitro* measurement of force were acquired from Nihon Kohden.

Muscle tissues processing and haematoxylin and eosin and modified Gomori trichrome staining for pathological analysis were performed as reported previously (Malicdan *et al.*, 2007). The stained sections were observed on a microscope (Olympus BX51, Olympus) and the images were acquired by DP70 digital CCD (Olympus). The number of rimmed vacuoles was counted on six 10-μm thick serial transverse cryosections with at least 100-μm interval of whole gastrocnemius muscle for each group of mice. For morphometric analyses, we stained the sarcolemma of muscle cryosections with anti-caveolin-3 antibody (Santacruz, 1:200 dilution) for 1 h followed by Alexa Fluor®-conjugated donkey IgG against goat IgG (Invitrogen, 1:800 dilution) for 30 min and imaged six randomly selected fields with a laser-scanning microscope (Olympus). Diameters of myofibres were measured from 600–800 fibres with ImageJ software (NIH). For quantifying the amount of amyloid deposits in myofibres, 10-μm thick cryosections of the gastrocnemius muscle were fixed in 4% paraformaldehyde for 10 min followed by immersion in ice-cold methanol for 10 min at −20°C and stained using a mouse antibody to mouse amyloid-β_{1-16} (6E10, Covance; 1:400 dilution) with an anti-caveolin-3 antibody. Digitized images at ×200 magnification were captured and used for analysis. Seven-μm thick cryosections from the gastrocnemius muscle were also stained using a rat antibody to mouse laminin-α2 (Alexis, 1:100) and either a mouse antibody to amyloid-β_{1-40} (Millipore, 1:300 dilution), a mouse antibody to amyloid-β_{1-42} (Millipore, 1:300 dilution) or a rabbit antibody to LC3 (Cell Signaling, 1:100 dilution). We applied appropriate secondary antibodies labelled with Alexa Fluor® dye according to the previous protocol (Malicdan *et al.*, 2007).

Samples for ELISA to measure amyloid-β_{1-40} and amyloid-β_{1-42} amounts in the gastrocnemius muscles were prepared according to the manufacturer's protocol with slight modifications. Muscle homogenates were extracted using equal volumes of 0.4% diethylamine and 100 mM NaCl. After centrifugation at 20 000*g* for 1 h at 4°C, the supernatant was neutralized with 0.5 M Tris base, pH 6.8. Amyloid-β_{1-40} and amyloid-β_{1-42} amounts were measured with ELISA kits for amyloid-β_{1-40} (IBL) and amyloid-β_{1-42} (IBL). The data were normalized with protein concentration.

After measurement of force, the mice were euthanized and the organs were harvested and immediately frozen on dry ice and kept at −80°C until use. The tissues were homogenized using a Potter homogenizer in a buffer containing 75 mM KCl, 10 mM Tris, 2 mM $MgCl_2$, 2 mM EGTA, and protease inhibitor mixture (Complete Mini Protease Inhibitor Tablet, Roche Applied Science), pH 7.4. The homogenized tissues were centrifuged for 1 h at 30 000*g* at 4°C. The pellet, which contained the membrane fractions, was used for measurement of the sialic acid and protein. After washing with the same buffer twice, the pellet was resuspended in 50 mM H_2SO_4, hydrolyzed and subjected to sialic acid measurement. We used the other pelleted fraction for analysis of the total protein amount by extracting protein with SDS buffer (2% SDS, 10% glycerol, 10 mM EDTA, 5% 2-mercaptoethanol, 0.0625 M Tris-HCl, pH 6.8).

We determined the activity of plasma creatine kinase, aspartate aminotransferase and alkaline phosphatase according to the manufacturer's protocol (Cicaliquid CK, AST and ALP, Kanto Chemical). We measured the blood urea nitrogen (BUN) level using a rate assay with urease and leucine dehydrogenase (Urutrateliquid BUN, Toyobo).

All values were expressed as means ± standard error (SE), or means ± standard deviation (SD) for plasma creatine kinase, aspartate aminotransferase, alkaline phosphatase and BUN values, as appropriate. For survival analysis, we used the Kaplan-Meier methods to draw the survival curve. For analysis of spontaneous locomotion activity, we used Wilcoxon's signed-rank test to compare the data recorded at 65, 72 and 80 weeks of age, respectively with that at 50 weeks in each mouse. For other analyses, we used one-way ANOVA with Dunnett's post-test or Kruskal-Wallis analysis with Dunn's post-test to compare the treatment group with non-treated group. A *P*-value of 0.05 was considered as the threshold for significance.

Results

We analysed the incorporation of sialic acid compounds into differentiated myotubes from a patient with GNE myopathy with increasing concentrations of NeuAc, ManNAc or 6'-sialyllactose. We found that the cellular sialic acid levels were similarly recovered by addition of any of those compounds to medium

(Fig. 1A). To analyse the pharmacokinetics of 6′-sialyllactose, we collected the blood and urine samples serially before and 5, 10, 30, 60, 120, 240 and 480 min after giving a single dose to mice via an intragastric route. After intragastric administration, 6′-sialyllactose appeared in blood within 5 min, peaked at 10 min, and returned to the baseline within 240 min (Fig. 1B). Large amounts of 6′-sialyllactose were excreted into urine at 60–120 min after administration, but it took 480 min for the 6′-sialyllactose to return to the baseline levelin urine, showing slower excretion into urine (Fig. 1C) than either NeuAc or ManNAc (Malicdan *et al.*, 2009). We also measured free NeuAc, which is the metabolized form of 6′-sialyllactose, and detected bipolar peaks in the blood at 5 and 60 min (Fig. 1D), while the peak was maximal in the urine at 120–240 min (Fig. 1E).

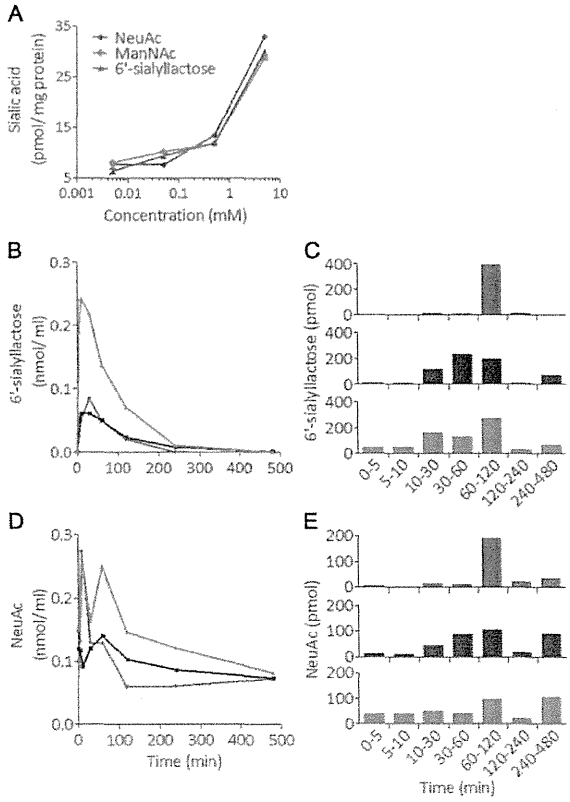

Figure 1 Comparison among compounds to increase cell sialylation and pharmacokinetics of 6′-sialyllactose. (**A**) Total sialic acid levels in myotubes from a patient with GNE myopathy treated with ManNAc, NeuAc and 6′-sialyllactose. Three compounds were added to condition medium at the concentration shown on the x-axis. (**B** and **C**) Phamacokinetics of orally administrated 6′-sialyllactose concentration in blood (**B**) and its excreted amounts in urine (**C**) before and at 5, 10, 30, 60, 120, 240 and 480 min after its oral administration. (**D** and **E**) Profiles of NeuAc concentration in blood (**D**) and its excreted amounts in urine (**E**). For the experiment of 6′-sialyllactose pharmacokinetics, three wild-type mice were used. Each colour (grey, blue, and red) denotes one mouse in **B–F**.

We conducted a preliminary NeuAc treatment study for symptomatic GNE myopathy mice and performed repetitive treadmill tests to assess their motor performance (Supplementary Fig. 1A). NeuAc treatment prevented the progression of symptoms on the loss of body weight and running performance of symptomatic GNE myopathy mice as compared to non-treated mice (Supplementary Fig. 1B and C), but this repetitive treadmill test led to physical exhaustion even in control littermates and increased mortality in the non-treated group (Supplementary Fig. 1A and C). Thus, in the next study, we measured voluntary running as a spontaneous locomotion activity to assess the motor performance to avoid causing further injury in symptomatic mice.

We analysed the progression of disease in GNE myopathy mice from 50 to 80 weeks of age. GNE myopathy mice were smaller than their littermates at 50 weeks of age, ranging from 28.6 to 32.5 g (Fig. 2A), and did not show body weight gain up to 80 weeks of age (Fig. 2B and Supplementary Fig. 2). Three (16.7%) of 18 GNE myopathy mice died by 80 weeks of age (Fig. 2C). Although marked variation in spontaneous locomotion activity was observed even in affected mice having the same genotype, control littermates maintained locomotion activity from 50–80 weeks of age (Fig. 2D). In contrast, GNE myopathy mice showed a decrease in activity with ageing, especially ~70–80 weeks (Fig. 2D and Supplementary Fig. 3B). At 80 weeks of age, the weight and cross-sectional area (CSA) of gastrocnemius and tibialis anterior muscles were smaller, and absolute isometric (P_t), tetanic (P_o) forces, and the size-normalized isometric force (P_t/CSA), tetanic force (P_o/CSA) of those muscles were markedly lower in GNE myopathy mice as compared to those of control littermates (Fig. 3A–F and Supplementary Fig. 5A–F), suggesting that the muscles were highly degenerated. Gastrocnemius muscles of 80-week-old GNE myopathy mice showed an increased number of atrophic fibres (Fig. 3G), accompanied by increased amyloid-β_{1-40} and amyloid-β_{1-42} deposits and LC3-positive rimmed vacuoles (Fig. 4A, D and E, and Supplementary Fig. 4) compared to previously characterized GNE myopathy mice at 55 weeks of age (Malicdan *et al.*, 2007, 2009). It should be noted that some of the GNE myopathy mice showed extremely numerous rimmed vacuoles (>300) in six muscle transverse sections at this age (Fig. 4B) (Malicdan *et al.*, 2009). The creatine kinase level was only mildly elevated; 80.5 ± 65.5 (mean ± SD, $n = 15$) versus 50.5 ± 11.7 IU/l ($n = 5$) (Supplementary Table 1).

For sialic acid supplementation in symptomatic mice, GNE myopathy mice at 50 weeks of age were divided into four groups: non-treated ($n = 18$), given water; low dose of 6′-sialyllactose at 100 mg/kg/d ($n = 10$); high dose of 6′-sialyllactose at 1000 mg/kg/d ($n = 8$); and NeuAc at 1000 mg/kg/d (NeuAc, $n = 11$). The treatment effect was measured by comparing the data from treated and non-treated mice with control littermates ($n = 15$).

In the high dose group, body weight was increased up to a level almost similar to that of the littermates during treatment (Fig. 2B). Such a body weight gain was not observed either in the low dose or NeuAc group (Fig. 2B). Mortality rate was almost equal among all the treated groups, as in this study, two to three mice in each of three treated groups died before the end of the study (Fig. 2C). Chronological examination of spontaneous locomotion activity revealed that the activity was well maintained in the high dose

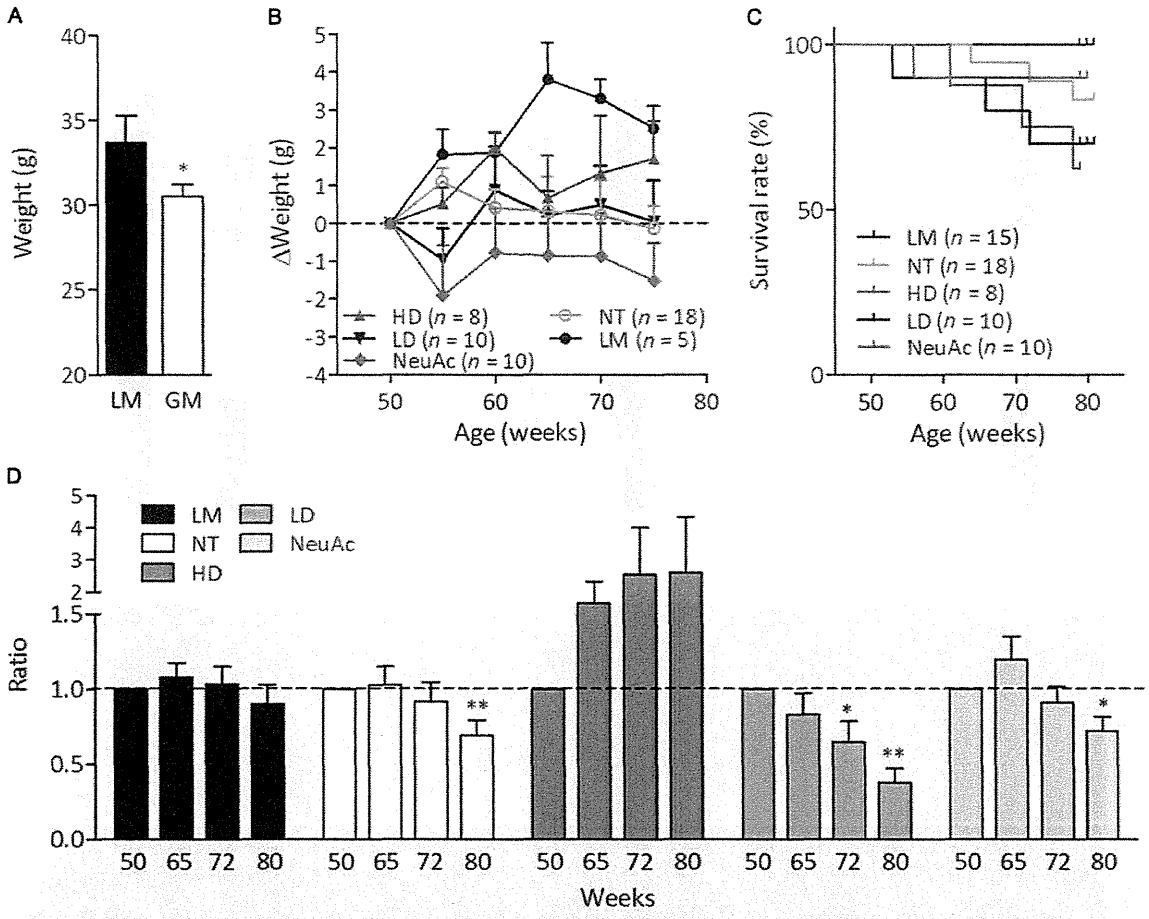

Figure 2 Phenotypes of treated and non-treated GNE myopathy mice. (**A**) Mean body weights of all GNE myopathy (GM) and littermate (LM) mice at 50 weeks of age. (**B**) Growth curves. The body weights at 55, 60, 65, 70, and 75 weeks of age are plotted relative to each at 50 weeks of age: GNE myopathy mice with high dose 6'-sialyllactose (HD, red upward closed triangles, $n = 8$); GNE myopathy mice with low dose 6'-sialyllactose (LD, blue downward closed triangles, $n = 10$); GNE myopathy mice with NeuAc (green closed diamonds, $n = 10$); non-treated GNE myopathy mice, non-treated (yellow open circles, $n = 18$); and control littermates (black closed circles, $n = 5$). (**C**) Survival curves: high dose (red), low dose (blue), NeuAc (green), non-treated (yellow) and littermates (black). (**D**) Spontaneous locomotion activities. The locomotion activities at 65, 72 and 80 weeks of age are plotted relative to those at 50 weeks of age: high dose (dark grey bars, $n = 5$), low dose (grey bars, $n = 7$), NeuAc (light grey bars, $n = 8$), non-treated (white bars, $n = 14$) and littermates (black bars, $n = 14$). $^*P < 0.05$, $^{**}P < 0.01$.

group (Fig. 2D), of which one mouse showed a marked increase (Supplementary Fig. 3C). A slight increase in activity was seen in the NeuAc group at 65 weeks of age (Fig. 2D), but by 80 weeks both low dose and NeuAc groups showed a significant decrease in locomotion.

Gastrocnemius muscle size in the high dose group at 80 weeks of age was increased up to the level of control littermates, while there was no change in the low dose and NeuAc groups (Fig. 3A and B). Likewise, tibialis anterior muscle size was increased to the level of littermates in the high dose group but not both in the low dose and NeuAc groups (Supplementary Fig. 5A and B). In terms of contractile properties, 6'-sialyllactose showed increases in twitch P_t and tetanic P_o forces of gastrocnemius muscle dose-dependently, and especially the high dose group presented increases in both muscle power beyond the levels of control littermates (Fig. 3C and D). Twitch force (P_t/CSA) and tetanic force (P_o/CSA) were also improved with 6'-sialyllactose in a dose-dependent manner, with a notable complete normalization in the high dose group (Fig. 3E and F). The NeuAc group showed mild improvement of P_o force and P_o/CSA (Fig. 3D and 4F), whereas P_t/CSA remained similar to the level of non-treated group (Fig. 3E). In the analyses of tibialis anterior muscles, we found a near-complete recovery of all contractile parameters in the high dose group (Supplementary Fig. 5). In the low dose group, twitch P_t and tetanic P_o forces were increased similar to the levels of control littermates in the absence of increase in muscle size, indicating a marked improvement of P_t/CSA and P_o/CSA. We did not observe any favourable results in the NeuAc group (Supplementary Fig. 5).

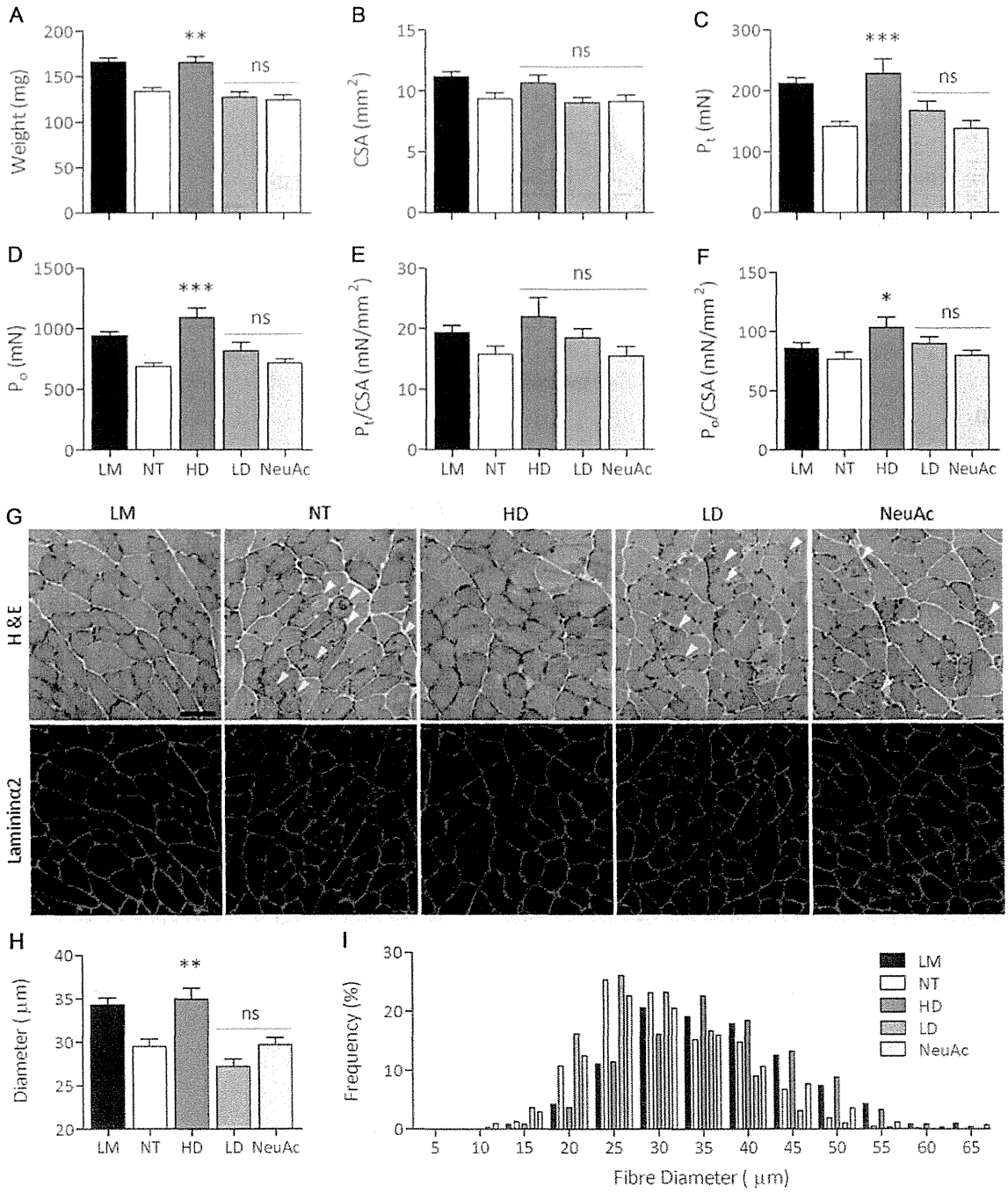

Figure 3 Muscle size and contractile properties of gastrocnemius muscle in GNE myopathy mice after 6'-sialyllactose treatment. (**A**) Muscle weight. (**B**) Whole-muscle CSA. (**C–F**) Contractile properties of the gastrocnemius: (**C**) isometric force (P_t), (**D**) tetanic force (P_o), (**E**) specific isometric force (P_t/CSA), and (**F**) specific tetanic force (P_o/CSA). (**G**) Haematoxylin and eosin staining and immunohistochemistry for laminin-α2 in transverse sections. Arrowheads denote rimmed vacuoles. Scale bar = 50 μm. (**H**) Mean diameters of myofibres after treatment. Control littermates (LM, black bars, $n = 14$); non-treated GNE myopathy mice (NT, white bars, $n = 15$); GNE myopathy mice with high dose 6'-sialyllactose (HD, dark grey bars, $n = 5$); GNE myopathy mice with low dose 6'-sialyllactose (LD, grey bars, $n = 7$); GNE myopathy mice with NeuAc (light grey bars, $n = 9$). (**I**) Histogram of myofibre diameters. High dose (HD, dark grey bars), low dose (grey bars), NeuAc (light grey bars), non-treated (white bars) and littermates (black bars). The histogram in high dose is shifted to the right, indicating the fibre size is increased after treatment. $^*P < 0.05$, $^{**}P < 0.01$, $^{***}P < 0.001$, ns = not significant.

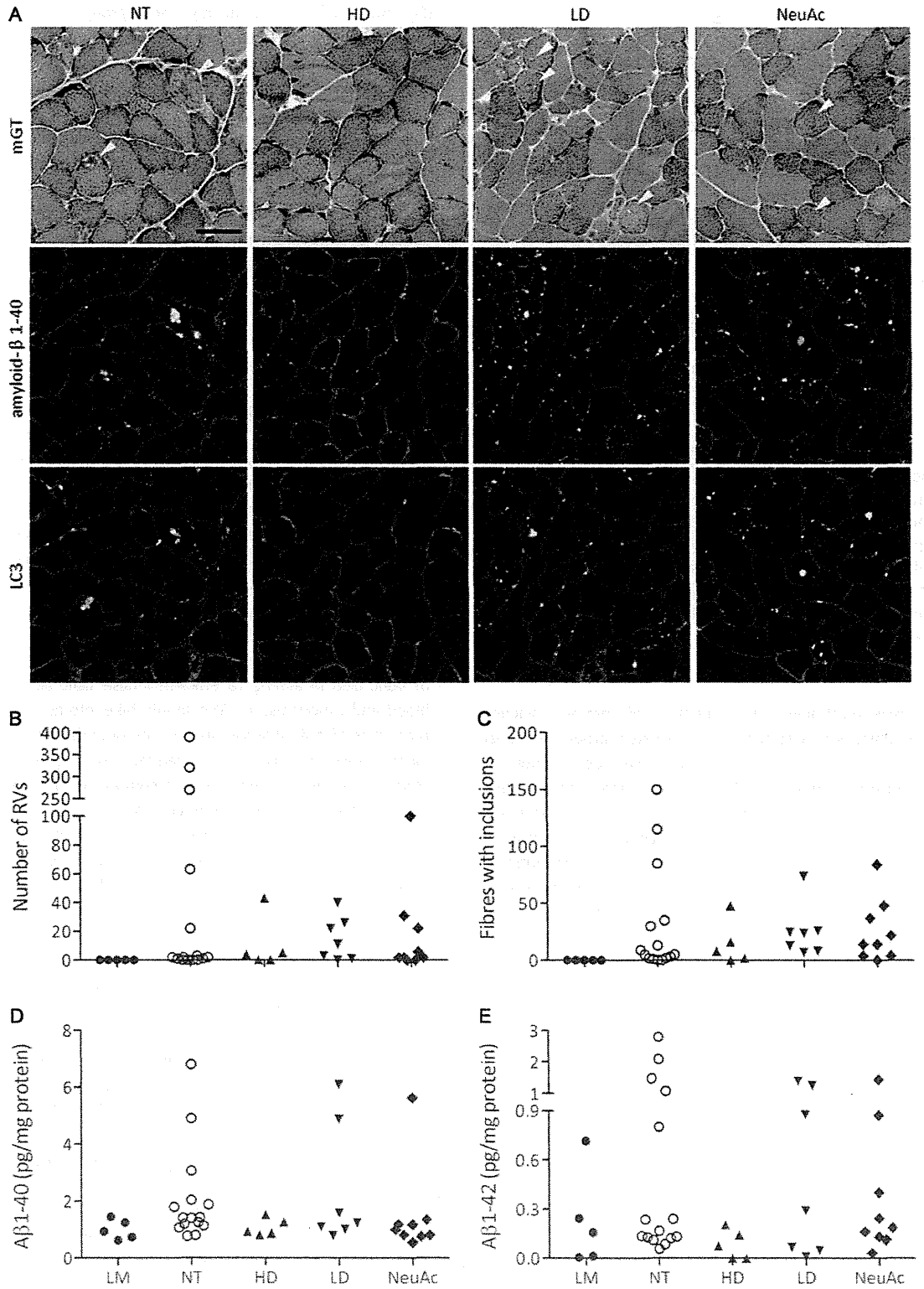

Figure 4 Number of rimmed vacuoles (RVs) and amyloid deposits after 6′-sialyllactose treatment. (**A**) Modified Gomori trichrome staining of gastrocnemius transverse sections. Arrowheads denote rimmed vacuoles. Immunosignals of amyloid-$\beta_{1\text{-}40}$ and LC3 are localized within rimmed vacuoles. Scale bar = 50 μm. (**B**) Number of rimmed vacuoles. (**C**) Amyloid inclusions. (**D** and **E**) Measurement of amyloid-$\beta_{1\text{-}40}$ (**D**) and amyloid-$\beta_{1\text{-}42}$ (**E**) in muscle by ELISA. Control littermates (LM, closed circles, $n = 5$); non-treated GNE myopathy mice, (NT, open circles, $n = 15$); GNE myopathy mice with high dose 6′-sialyllactose (HD, upward closed triangles, $n = 5$); GNE myopathy mice with low dose 6′-sialyllactose (LD, downward closed triangles, $n = 7$); GNE myopathy mice with NeuAc (closed diamonds, $n = 9$).